Neurochemistry-enriched dynamic causal models of magnetoencephalography, using magnetic resonance spectroscopy

Amirhossein Jafarian[1], Laura Hughes[1,2], Natalie E Adams[1], Juliette Lanskey[2], Michelle Naessens[1], Matthew A Rouse[1,2] , Alexander G Murley[1], Karl J Friston[3], James B Rowe[1,2]

[1] Department of Clinical Neurosciences and Cambridge University Hospitals NHS Trust, University of Cambridge, United Kingdom

[2] MRC Cognition and Brain Sciences Unit, University of Cambridge, Cambridge, UK

[3] The Wellcome Centre for Human Neuroimaging, UCL Queen Square Institute of Neurology, United Kingdom

Contribution:

Amirhossein Jafarian: Conceptualization, Methodology, Software, Validation, Formal analysis, Writing Original Draft, Data Curation, Visualization.
Laura Hughes: Max-filtering software, Review & Editing.
Natalie E Adams: Discussion, Review & Editing.
Michelle Naessens: Data collection, Review & Editing.
Matthew A Rouse: Data collection, Review & Editing.
Juliette Lanskey: Discussion, Review & Editing.
Alexander G Murley: MRS Data Collection, Review & Editing.
Karl J Friston: Conceptualization, Methodology, Review & Editing, Supervision.
James B Rowe: Conceptualization, Methodology, Review & Editing, Supervision, Funding acquisition.

Correspondence: Professor James B Rowe

Cambridge Centre for Frontotemporal Dementia
Department of Clinical Neurosciences
University of Cambridge
Herchel Smith Building, Forvie Site
Robinson Way, Cambridge Biomedical Campus,
Cambridge,
CB2 0SZ, UK

Abstract:

We present a hierarchical (i.e., empirical) Bayesian framework for testing hypotheses about synaptic neurotransmission, based on the integration of ultra-high field magnetic resonance spectroscopy (7T-MRS) and magnetoencephalography. A first level dynamic causal modelling of cortical microcircuits is used to infer the connectivity parameters of a generative model of neurophysiological observations. At the second level, 7T- magnetic resonance spectroscopy (MRS) estimates of regional neurotransmitter concentration supply empirical priors on synaptic connectivity. We compare the evidence for alternative empirical priors, defined by monotonic functions of spectroscopic estimates, on subsets of synaptic connections. For efficiency and reproducibility, we used Bayesian model reduction, parametric empirical Bayes and variational Bayesian inversion. In particular, we used Bayesian model reduction to compare models of how spectroscopic neurotransmitter measures inform estimates of synaptic connectivity. This identifies the synaptic connections that are influenced by neurotransmitter levels, as measured by 7T-MRS . We demonstrate the method using resting-state magnetoencephalography (i.e., task-free recording) and 7T-MRS data from healthy adults. We validate the analysis by split-sampling of the magnetoencephalography dataset. Our results confirm the hypotheses that GABA concentration influences local recurrent inhibitory intrinsic connectivity in deep and superficial cortical layers, while glutamate influences the excitatory connections between superficial and deep layers and connections from superficial to inhibitory interneurons. The method is suitable for applications with magnetoencephalography or electroencephalography, and is well-suited to evince the mechanisms of neurological and psychiatric disorders, including responses to psychopharmacological interventions.

Keywords: Dynamic causal modelling, canonical microcircuits, Bayesian model reduction, parametric empirical Bayes, magnetoencephalography, magnetic resonance spectroscopy.

1 Introduction

This paper introduces an empirical Bayesian methodology for inferring synaptic physiology from human *in vivo* neurophysiological recordings and *in vivo* measurements of neurochemicals, including neurotransmitters. It is an example of a broader class of enriched dynamic causal models (DCMs), informed by multimodal data that could incorporate neurochemistry, molecular pathology or selective loss of neuronal sub-populations and their synapses. Magnetic resonance spectroscopy (MRS) can be used to estimate individual differences in key neurochemical concentrations in local brain regions (Blüml and Panigrahy, 2012). It has been used to quantify neurochemical changes in neurological and neuropsychiatric disorders, such as Alzheimer's disease (Wang et al., 2015), frontotemporal lobar degeneration-related syndromes (Murley et al., 2020, Murley et al., 2022), and schizophrenia (Jelen et al., 2018, Cohen et al., 2015, Duarte and Xin, 2019), as well as normal aging (Boumezbeur et al., 2010). Such spectroscopy can be predictive of task performance and the response to pharmacological interventions (Chowdhury et al., 2012, Stagg et al., 2011, McColgan et al., 2020, Gawne et al., 2020, Schmitz et al., 2017, Adams et al., 2021). Differences in neurotransmitter levels influence synaptic transmission, which in turn affect the generators of magneto- and electro-encephalographic signals (M/EEG).

Here, we characterise the relationship between physiology and neurotransmitter levels, using a hierarchical Bayesian approach (Friston et al., 2016). We present a method for specifying and comparing the evidence for hierarchical models (using parametric empirical Bayes) that encodes the effect of neurotransmitter levels (as measured with MRS) on different combinations of synaptic parameters in a neural mass model of MEG recordings. Our approach complements previous studies, where correlational analysis has been used to investigate relationships between spectroscopy measures and electrophysiology (Rideaux, 2021, Steel et al., 2020, Kober et al., 2001). We envisage that our method may be useful for characterising the synaptic deficits in several neuropsychiatric conditions e.g., (Adams et al., 2021, Limongi et al., 2021).

MRS is non-invasive neuroimaging modality that captures signature of biochemical concentrations, including the neurotransmitters glutamate (GLU) and gamma-aminobutyric acid (GABA) (McColgan et al., 2020, Stagg and Rothman, 2013). Glutamatergic

neurotransmission mechanisms include release, reuptake into astrocytes, conversion to glutamine then glutamate, then vesicular repacking (Gruetter et al., 2001, Pellerin et al., 2007, van der Graaf, 2010). In contrast, GABA cycling is predominantly neuronal where, following a release phase, there is presynaptic GABA reuptake and vesicular repackaging (Gruetter et al., 2001). The majority of GABA and glutamate is intracellular (Myers et al., 2014) but even total GABA and glutamate concentrations have been reported to correlate with neurophysiological features such as gamma oscillatory power and corticospinal excitability (Lally et al., 2014, Greenhouse et al., 2017).

In what follows, we show that neurotransmitter levels can be used as prior constraints on the estimation of effective synaptic connectivity, in biophysically informed models of cortical function. For example, glutamate and GABA concentrations control the dynamics of the excitatory amino-3-hydroxy-5-methyl-4-isoxazolepropionic acid (AMPA) receptors and inhibitory GABAergic receptors respectively (Rideaux, 2020, Gruetter et al., 2001). The aim of the current work was to compare the evidence for alternate hypotheses regarding the relationships between glutamate/GABA concentrations and synaptic connectivity, quantified using non-invasive MRS recordings and M/EEG data, respectively.

The first step in establishing this relationship is to infer synaptic parameters from neurophysiological observations. We use Dynamic Causal Modelling (DCM) to invert a canonical microcircuit model of resting state magnetoencephalography in healthy adults (Friston et al., 2012, Friston et al., 2003). Dynamic causal modelling entails the variational Bayesian inversion of biologically-informed forward models of neurophysiological observations, under the Laplace assumption (Friston et al., 2007). In DCM, gradient optimization of variational free energy is used for approximating the posterior probability density over unknown model parameters, and the model evidence (i.e.. The marginal likelihood) (Friston et al., 2007, Friston et al., 2008). The free energy provides a lower bound on log-model evidence, which represents the model accuracy adjusted for complexity. Model evidence associated with alternate hypotheses—about the underlying generators of the magnetoencephalographic data—are compared using Bayesian model reduction. This identifies the most likely explanation for the empirical data (Kass and Raftery, 1995, Friston, 2011, Friston et al., 2011, Jafarian et al., 2019). Crucially, Bayesian model reduction (BMR) enables the computationally efficient evaluation of posteriors and model evidence under a

reduced prior; i.e., a model specified in terms of new prior constraints (Friston et al., 2018, Friston and Penny, 2011). We estimate the parameters and evidence for a full model of a given dataset and then use BMR to evaluate posteriors and model evidences under alternative priors (Friston and Penny, 2011, Friston et al., 2019).

At the second (e.g., group) level, hierarchical or parametric empirical Bayes (PEB) allows one to include empirical priors of interest (Friston et al., 2015, Friston et al., 2016). Usually, second level models apply priors that are conserved over multiple participants. This means the first level corresponds to a within-subject analysis, while the second level is a between-subject or group analysis (using subject specific posterior estimates furnished by the first level). The combined hierarchical model can then be assessed in terms of its evidence, and subject to BMR to test different hypothesis at the within or between-subject level.

In this paper, we compare the evidence for different hypotheses about the association between MRS estimates of neurotransmitter concentration and synaptic function. For a given set of connections, we use a hierarchical optimization (a greedy search followed by a constrained optimization) to identify the (linear or nonlinear) function of the MRS estimates—furnishing prior constraints—that maximises model evidence at the group level. We then use model reduction to determine which subsets of synaptic parameters are sensitive to individual differences in neurotransmitter concentration. This approach complements previous work by (Stephan et al., 2009, Sokolov et al., 2019) who used diffusion-weighted imaging tractography to furnish empirical priors on connectivity parameters from functional magnetic resonance imaging time series. However, unlike previous work, we do not assume a one-to-one relation between MRS measures and connections in the generative model. Rather, we seek evidence to find which synaptic connections are informed by the empirical measures.

In the following sections, we describe the multi-modal dataset (magnetoencephalography and 7T-MRS) and the first-level DCM used to fit cross-spectral density data features. We then describe the second (group) level PEB model of the mapping between neurotransmitter concentration and synaptic physiology. We present the results of first-level and group-level DCMs, using MRS data as empirical priors. Finally, we discuss the potential applications and limitations of the method. A glossary and definitions of acronyms and variables used in this paper are provided in Tables 1 to 4.

2 Material and Methods

2.1 Participants

Eleven healthy adults (age 63-77 years, five women) participated after providing written informed consent. The study had ethical approval from the Cambridge 2 Research Ethics Committee. They were free from neurological or major psychiatric disorders and took no regular medication. Each participant underwent 7T MRI and MRS (Murley et al., 2020) and task free resting-state magnetoencephalography, on separate days.

2.1.1 7T MRS data

Ultrahigh field magnetic resonance data were acquired using a Siemens Terra scanner at the Wolfson Brain Imaging Centre using short-echo semi-LASER sequence (repetition time/echo time = 5000/26 ms, 64 repetitions (Deelchand et al., 2015)), and VAPOR water suppression calibration (Gruetter and Tkáč, 2000). A 2cm isotropic cubic voxel was located over the right inferior frontal gyrus (IFG). The details of the MRS processing have been reported previously in (Murley et al., 2020, Murley et al., 2022). In brief, the spectra were pre-processed to remove effects of eddy currents and frequency/phase shifts using MRspa (Dinesh Deelchand, University of Minnesota, www. cmrr.umn.edu/downloads/mrspa). The LCModel method (Version 6.2-3) was used to quantify glutamate and GABA between 0.5 and 4.2 ppm (Provencher, 1993). A MP2RAGE sequence (repetition time =4300 ms, echo time = 1.99 ms, resolution = 99 ms, bandwidth= 250 Hz/px, voxel size = 0.75 mm3, field of view =240240157 mm, acceleration factor (A>>P) = 3, flip-angle = 5/6 and inversion times = 840/2370 ms) was acquired for co-registration and segmentation, using SPM12 for partial volume correction, from fractions of grey matter, white matter and CSF. A generalized linear model was used to remove the effect of age, sex and partial volume. Residual glutamate and GABA values were used for subsequent analysis.

2.1.2 MEG data:

Resting state MEG data were collected during two recordings, each of five minute duration, on a different day to the MRS, with eyes closed using an Elekta Vector View system with 204 planar gradiometers and 102 magnetometers. MEG data were recorded continuously with

1000 Hz sampling rate. Participants' horizontal and vertical eye movements were recorded using bipolar electro-oculogram and electro-cardiogram electrodes. Five head position indicator coils were placed on an EEG cap to track the head position. Three fiducial points (nasion, left and right pre-auricular) and a minimum of 100 head shape points were digitised using Polhemus digitization.

The data were pre-processed using the Elekta Neuromag toolbox (Elekta Oy), with MaxFilter v2.2.12 for detection and interpolation of bad sensors, signal space separation to remove external noise from the data and head movement correction. The data were then high-pass filtered at 1 Hz, stop-band filtered around [22 to 24] Hz and [47 to 51] Hz and divided into epochs of one second duration. We used the Field trip Toolbox (Oostenveld et al., 2011) for detection and removal of eye movement artefacts and discontinuities.

We applied empirical Bayesian inversion in SPM12 for source inversion and extraction of the right IFG source timeseries for subsequent analyses (Litvak et al., 2011). We concatenated the data of the two recordings and then divided the source data into two sets, one comprising the odd numbered epochs ('odd-Data') and one with the even numbered epochs ('even-Data') for each participant to assess the reliability of the results (Litvak et al., 2015). We separately averaged power spectral responses of the odd and even datasets. The two power spectral densities (referred to as Odd-PSDs and Even-PSDs) are used as the data features in the DCM of cross-spectral density.

2.2 First level analysis using dynamic causal modelling of resting states MEG data

To infer the neurophysiological parameters generating observed resting state MEG data, we used "DCM for cross spectral density" in SPM12 (Friston et al., 2012, Moran et al., 2007, Moran et al., 2011). Spectral features in the resting state MEG were used to infer synpatic parameters of a biophysically-informed neuronal mass model, together with model evidence. DCM for cross spectral density assumes that recorded electrophysiological oscillations are due to finite responses of neuronal dynamics, under endogenous random fluctuations (Basar et al., 2012, Haken, 1977).

We used a conductance based neuronal mass model as shown in Figure 1: known as "CMM_NMDA" model in DCM/SPM12 (Moran, 2015, Moran et al., 2013, Shaw et al., 2017). The CMM_NMDA model represents the actvity of cortical columns based on the interactions of four neuronal populations: excitatory spiny stellate cells, superfical pyramidal cells, inhibitory interneurons, and deep pryramidal cells as shown in Figure 1.

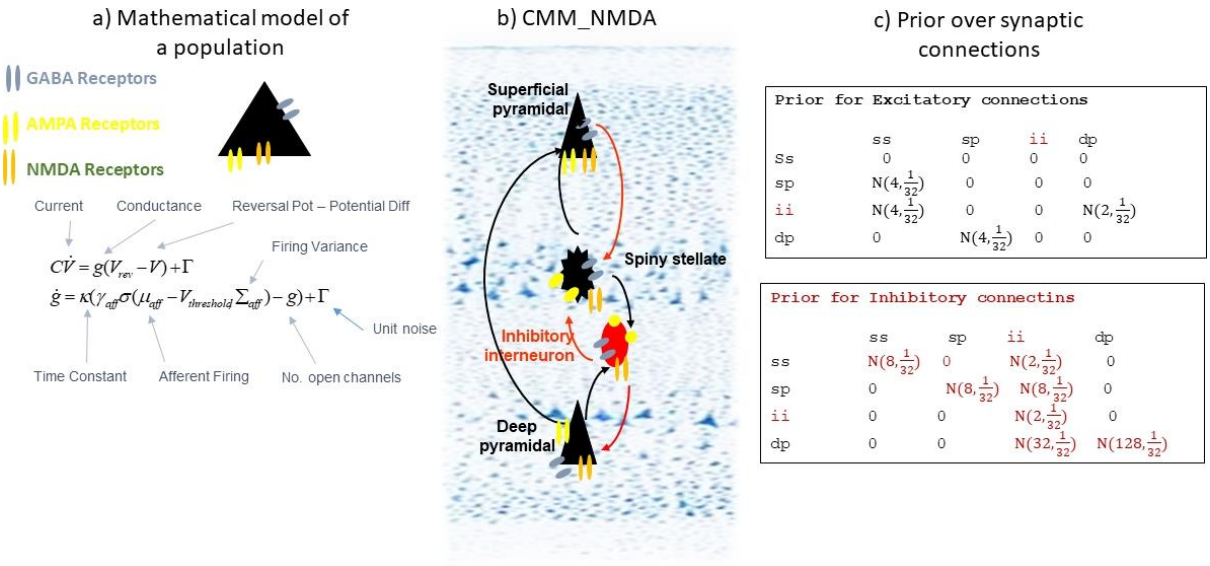

Figure 1. Conductance based neural mass model (middle figure (b)), CMM_NMDA model. A cortical column is divided into three layers, the dynamics of each of which is captured by Morris-Lecar model (left hand panel (a)): Superficial (sp) and deep pyramidal (dp) cells are in the top and bottom of the layers, respectively. Excitatory interneurons (spiny stellate cells, ss) are located in layer four. Inhibitory interneurons (ii) are distributed across all layers and are modelled using one population that interacts with all other populations. In addition, each population is equipped with a self-inhibition which assures dynamical stability around a stable fixed point. Prior probability distribution of the laminar connections in DCM are shown in panel (c). An element of ij (i row and j column) in each matrix shows a connection that originates at population indexed by j and projects to a population indexed by i (zero value implies no connections).

Each population is represented by a Morris–Lecar model (Moran et al., 2013). The dynamics of each population is govened by stochastic differential equations that emulate the dynamics of pre/post-synaptic potentials, firing rates and membrane conductances. The dynamics of membrain potentials, V, and conductances of an ion channel, g_*, are govered by the following equations:

$$\frac{dV}{dt} = \frac{1}{C}[g_L(V_L - V) + g_{AMPA}(V_{AMPA} - V) + g_{GABA}(V_{GABA} - V) + g_{NMDA}\, m(V)(V_{NMDA} - V)] + u, \qquad (1)$$

$$\frac{dg_*}{dt} = \frac{1}{\tau_*}\left(\sum_{k=sp,inh,dp,ss} H_k\, \sigma_k - g_*\right) + u, \qquad *= [L, AMPA, GABA, NMDA]$$

In equation 1, C is the membrane capacitance, u is random endogenous fluctuation, L is passive leak current where its conductance is constant, g_* is conductance associated with ion channels/receptors with time constant τ_*, $V_{AMPA,GABA,L,NMAD}$ are the reversal equilibrium potentials of the ion channels. The $m(V)$ in equation 1 is the actvity-dependent magnesimum channels which is given by $m(V) = \frac{1}{1+0.2\, exp(-\alpha_{NMDA}\, V)}$. The term σ_k in the equation 1 is the non-negative afferent presynaptic firing from population k, which is scaled by afferent intrinsic connectvity H_k.

The scaled presynaptic firing rates are a proxy for neurotransmitter levels measured by MRS. Therefore, we hypothesise a relation between the MRS GLU/GABA measures and excitatory and inhibitory H_k connections, which scale presynaptic actvity. In other words, the MRS GLU/GABA can be used as an empirical prior on excitatory/inhibityory connections in the generative model.

Mathamtically the temporal dynamics of the conductance based model can be written in the canonical form of a dynamical system as follows (Friston et al., 2012):

$$\dot{x} = f(x, \theta) + u(\theta) \qquad (2)$$

Where θ denotes a vector of all unknown parameters (i.e., H_k, $\tau_.$), x is the state of neuronal populations in the model, $f(x, \theta)$ is a function that is the concatenated version of the right hand sides of the equation 1—over all populations—and u represent endogenous fluctuations, conventionally modelled by (structured) pink noise. The noise in equation 2 has a cross-spectrum $g_u(\omega, \theta) = FT(E[u(t), u(t - \tau)])$: Please see Table 2.

One can approximate the dynamics of equation (2) with the (first order) linearised model $\dot{x} = (\nabla_{x^*} f_\theta)x + u$ (∇_{x^*} denotes the Jacobian at x^*) with the spectral response:

$$K(\omega,\theta) = FT\ (\exp \tau . \nabla_x f(x,\theta)) \quad (3)$$

Given the spectral response of the system, the generative model of neuronal activity, $g_x(\omega)$, can be calculated as follows:

$$g_x(\omega) = K(\omega,\theta).\, g_u(\omega,\theta).\, K(\omega,\theta)^T + g_o(\omega,\theta) \quad (4)$$

In equation 4, $g_o(\omega,\theta)$ represents the spectrum of the observation noise, which is a sum of common and source specific noise. The spectral response in sensor space can also be generated by inclusion of a forward electromagnetic model into equation 4, which is denoted by $L.M(\omega)$ (L is the gain and M is the head model), as follows:

$$g_y(\omega) = L.M(\omega).\, g_x(\omega,\theta).\, M^T(\omega).\, L^T + \epsilon \quad (5)$$

In equation 5, $g_y(\omega)$ is the cross spectra of the MEG data and $\epsilon \sim N(0,\sigma)$ is a random effect (with unkown covariance). Because we perform the DCM in source space, the forward electromagnetic model in this case just applies a scaling parameter.

The unkown parameters in the DCM are specified as log-scale values. This means that the parameter vector in DCM is a random variable, which is given by $\theta = \theta_0 \exp(\hat{\theta})$. Here, θ_0 is a biologically informed scaling for the parameter and $\hat{\theta}$ is a random variable, with prior normal density $\hat{\theta}_0 \sim N(0, \sum_\theta)$ of zero mean and covariance $\sum_\theta$. This expresses the belief about the range over which parameters can vary. Note that scale parameters of this sort cannot be less than zero; for example, distances and lengths or rate and time constants or precisions and variances.

2.3 Second level analysis: group DCMs informed by empirical priors

In many translational neuroscience studies, the goal is to test hypotheses at the group level, where subject-specific information is given by summary statistics. In PEB, this subject specific information is the posterior over key model parameters at the first level (Zeidman et al., 2019a, Zeidman et al., 2019b, Friston et al., 2015, Friston et al., 2016). At the second level the

objective is to test whether synaptic connections depend on between subject variables, such as age, disease-severity, genetics, DTI, MRS, etc (Friston et al., 2016). In other words, PEB seeks to explain intersubject variability on one or more first level model parameters.

Mathematically, we denote a vector of model parameters at the first level DCM, over all participants, by a column vector $\theta^{(1)}$ with dimension $np \times 1$ (n number of participants and p is the number of parameters for each participant). Then the generative model at the second level (i.e., random effects on the parameters) is given by (Friston et al., 2016):

$$\theta^{(1)} = (X \otimes I)\theta^{(2)} + \epsilon^{(2)} \tag{6}$$

Where $X \in R^{n \times r}$ is the design matrix with $r \geq 1$ covariant (the first regressor of X is always equal to one and reflects the group mean). The symbol $\otimes$ is the Kronecker product and I is the $p \times p$ identity matrix. The random effects have a Gaussian distribution $\epsilon^{(2)} \sim N(0, \Pi^{(2)})$ (where $\Pi^{(2)}$ is precision matrix or inverse of covariance). The precision matrix is parameterized with a single (hyper-precision) parameter, γ, as follows (Friston et al., 2016):

$$\Pi^{(2)} = I_S \otimes (Q_0 + e^{-\gamma}\, Q_1\,) \tag{7}$$

In equation 7, $Q_0 \in R^{p \times p}$ is the lower bound on the precision, defined with a small positive value). The (hyper)parameter, γ, scales a precision matrix $Q_1 \in R^{p \times p}$, which is (by default) 16 times the prior precision of the group mean (Zeidman et al., 2019b): this hyperprior ensures that random effects are small in relation to prior uncertainty about the parameter in question.

The critical question is whether an alternative prior increases or decreases model evidence (Friston et al., 2016). This is an optimisation problem, where the objective function is the free energy of the PEB model. Inversion of the hierarchical model is computationally expensive if all parameters of the first level need to be inferred every time the second level parameters change (Raman et al., 2016). However, BMR can be used to re-evaluate first level posteriors

under updated second level parameters (Friston et al., 2016, Litvak et al., 2015). This significantly improves the efficiency of inversion for PEB models.

2.4 Investigating relation between MRS and synaptic connections:

2.4.1 Problem setting:

We test whether excitatory and inhibitory synaptic connections depend on (i.e., are functions of) glutamate and GABA measures, respectively. We used PEB to specify and compare the evidence for different functions of MRS measures, as illustrated in Figure 2.

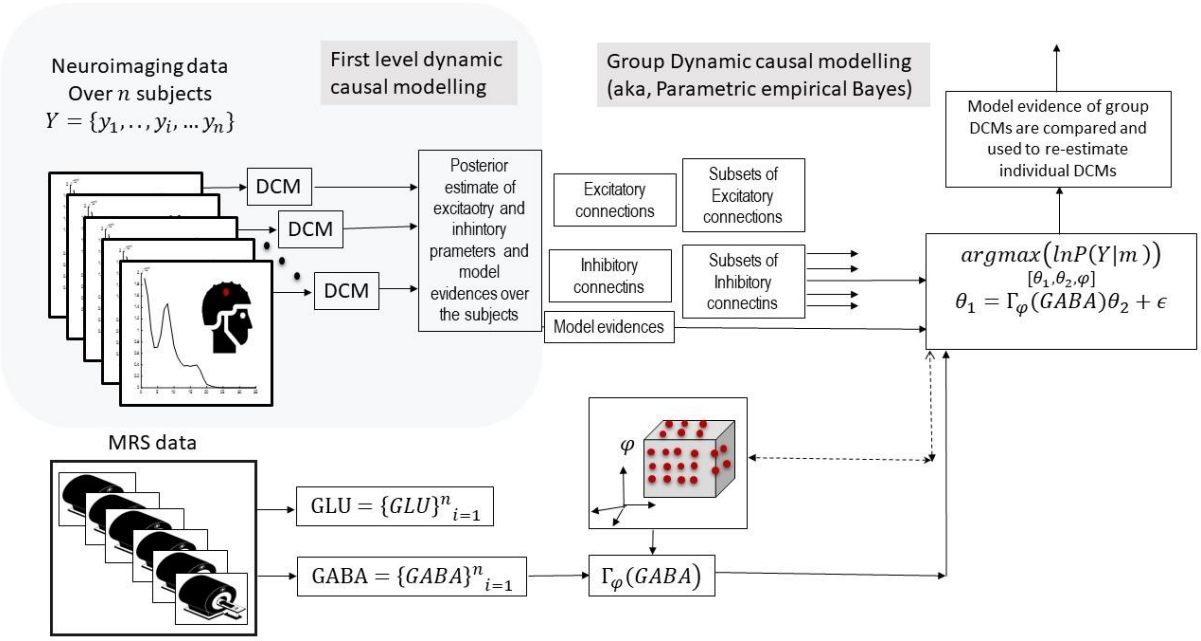

Figure 2. MRS informed group DCM for MEG. This graphic illustrates a group DCM (aka PEB model) inversion using MRS data as empirical priors. First level DCM (left side of panel) infers synaptic physiology from each participants' data. A function of MRS GLU or GABA (bottom panel) measures are considered as empirical priors for certain parameters in the group DCM (right panel). Bayesian model reduction evaluates the effect of empirical priors and evaluates the model evidence for the group DCM. The objective is to find the optimal function of MRS measures—that inform synaptic parameters in the CMM-NMDA model—by maximising PEB model evidence. Image credit for MRI scanner by Grant Fisher, TN from the Noun Project, CC BY 3.

To identify which synaptic parameters were sensitive to neurotransmitter levels, we grouped the inferred synaptic connections into excitatory and inhibitory subsets. In detail, for the l_{EX} (l_{Inh}) excitatory (inhibitory) connections in the CMM_NMDA model, we define $2^{l_{ex}}$ -1 ($2^{l_{Inh}} - 1$) different possible combinations. The ensuing subsets of the connections (over all

participants) are considered as the dependent variable of the PEB model (i.e., the right-hand side of equation 1). This model encodes a hypothesis about the relationship between (each subset of) connections, $\phi^{(1)} = \{\phi_i\}^k{}_{i=1}$ and a particular function of MRS data: $\Gamma_\varphi(MRS)$ (where Γ is a smooth and monotonic function with unknown parameters, φ), which can be expressed as follows:

$$\phi^{(1)} = \left([1\ \Gamma_\varphi(MRS)]\ \otimes I\right)\phi^{(2)} + \epsilon^{(2)} \tag{8}$$

In equation 8, there are two sets of unknowns that need to be inferred; namely, *(i)* the subset of connections $\phi^{(1)}$ and *(ii)* the function or map $\Gamma_\varphi(MRS)$. These unknowns are the hyper-parameters in equation 6. To find optimal hyperparameters, we recursively select subsets of synaptic connections and estimate the MRS function parameters, such that the model evidence in equation 6 is maximised. In other words, for any combination of synaptic parameters, we seek the MRS-informed PEB model with the highest evidence, using BMR. This allows us to identify the most likely relationship between synaptic parameters and MRS data.

To cross-validate the results, we separately tested the relationship between inferred synaptic parameters and MRS by splitting the data into odd and even numbered magnetoencephalography epochs (odd-Data and even-Data). The ensuing procedure is shown in Figure 3.

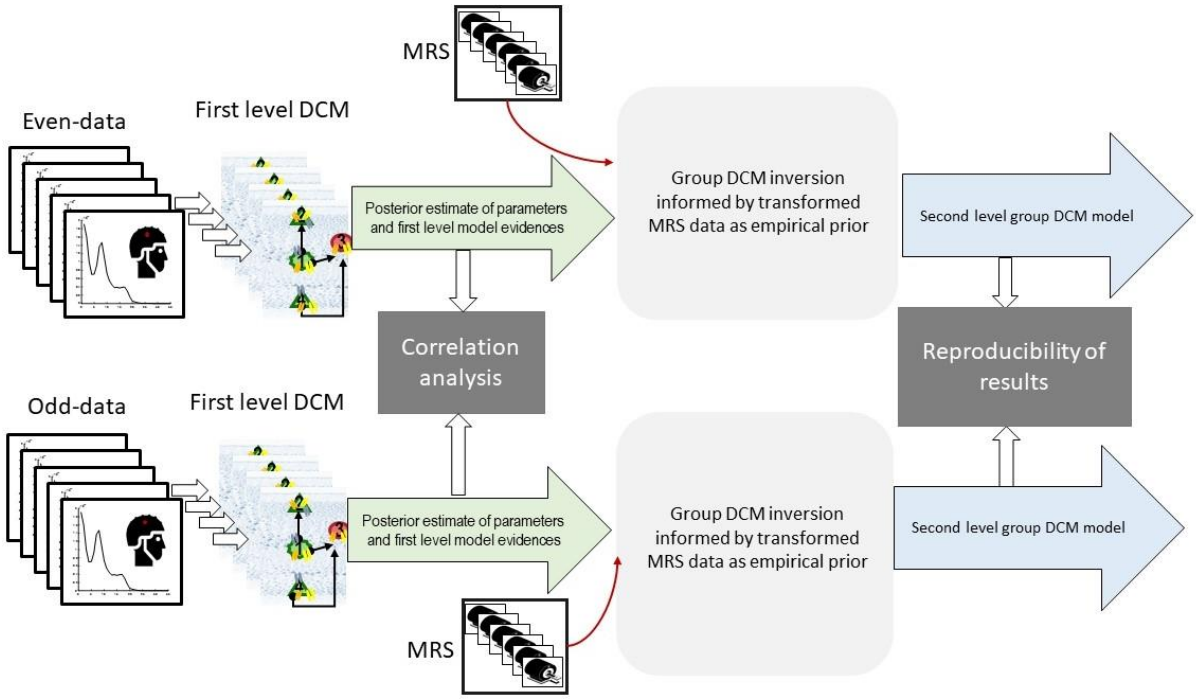

Figure 3.Reproducibility-check procedure. The MEG data for each participant is divided into two separate datasets, 'odd-Data' and 'even-Data'). DCM for MEG is used to infer synaptic parameters for each. A post hoc correlation analysis is used to test agreement between the ensuing estimates. Parameter estimates that are consistent over the datasets are considered for further analysis. We perform the group level inversion informed by MRS data for odd and even datasets on the selected parameters and explore which sets of connections are best informed by a function of MRS data. Finally, we compare the outcome of the PEB inversion and check the consistency of the results between the odd-Data and even-Data. Image credit for MRI scanner by Grant Fisher, TN from the Noun Project, CC BY 3.

2.4.2 Functional form of the empirical MRS priors:

The functional form of the MRS mapping is not known *a priori*. We therefore limit the search space over the MRS transformations to continuous and monotonic polynomial maps and sigmoid nonlinear functions, which cover a wide range of linear and nonlinear forms. The class of polynomials provides an approximation (Bishop, 2006) to any nonlinear monotonic form (Spivak, 2020):

$$\Gamma_{\varphi}(MRS) = \sum_{i=1}^{n} \phi_i (MRS)^i \qquad (9)$$

Here, ϕ_i are n unknown hyperparameters that need to be inferred by finding the values that maximise model evidence. This class of functions express different nonlinear relations including saturations (Stephan et al., 2009, Stefanovski et al., 2019), $n = 1$ implies a linear transformation of the MRS data.

Animal experiments suggest that changes in GABA and GLU concentrations are related to neuronal responses via a sigmoid relationship (Benardete and Kriegstein, 2002, Dyke et al., 2017, Chebib et al., 2009). The general form of a sigmoid nonlinearity can be parameterised as follows:

$$\Gamma_{\varphi}(MRS) = \frac{1}{1 + \exp(-\varphi_1(MRS - \varphi_2))} \tag{10}$$

Here, the unknown hyperparameters φ_1, φ_2 are the slope and threshold parameters of the sigmoid transformation, respectively.

2.4.3 Hyperparameter estimation:

To estimate unknown hyperparameters, we first sorted the MRS measures from small to large values, which defined an interval of the real line (called the domain of the MRS data). We then examined the variation of the parameters under the MRS transformation. In the case of the polynomial form, we checked the monotonicity of the transformation. More formally, we denoted the space of monotonic functions by $\aleph$, and defined the function γ over the ordered domain set of the MRS data to identify the range for the variation of the parameters in the polynomial function. This function has the following properties:

$$\gamma: [\min(MRS), \max(MRS)] \rightarrow R$$

$$\gamma_{\varphi}(.) \in \aleph \ , \quad \varphi \in \left[\min(\varphi_1) : \Delta_{\varphi_1} : \max(\varphi_1)\right] \times \ldots \times \left[\min(\varphi_n) : \Delta_{\varphi_n} : \max(\varphi_n)\right] \tag{11}$$

$$\gamma_{\varphi}(MRS) = \Gamma_{\varphi}(MRS)$$

Each parameter in the γ map, φ_i, varies with resolution (or step-size) Δ_{φ_i}. Note that γ_φ and Γ_φ have the same functional forms but with continuous and discretised domains. Having established the appropriate ranges (see Table 4), we used a hierarchical scheme to estimate the parameters of the map, $\Gamma_\varphi(MRS)$. For each set of synaptic connections, we calculated the model evidence—using BMR—for different values of the hyperparameters over the interval $\left[\min(\varphi_1) : \Delta_{\varphi_1} : \max(\varphi_1)\right] \times \ldots \times \left[\min(\varphi_n) : \Delta_{\varphi_n} : \max(\varphi_n)\right]$. This constitutes an exhaustive grid search. This was followed by a constrained Newtonian search, within the neighbourhood of the selected grid point, to identify the precise value of the hyperparameters that maximised model evidence. We repeated this hyperparameter optimization over all possible subsets of the synaptic connections and selected the combinations with the greatest model evidence.

3 Results:

3.1 DCM for MEG:

The spectral activity from both data sets per participant (even-Data and odd-Data) are used as the data features for a conventional "DCM cross spectral density" to infer the parameters of the canonical microcircuit (CMC_NMDA). The predicted and observed data are provided in the supplementary material. By comparing the goodness of fit of the DCM, one can ensure the model inversion has not been trapped in local minima. The comparison of predicted and observed spectral data shows that the synaptic parameter estimates can replicate the spectral patterns of both even-Data and odd-Data; with an example shown in Figure 4 (see the supplementary material for the remaining comparisons). The correlation between the free energies associated with DCM inversions of odd/even PSD data is shown in Figure 4.

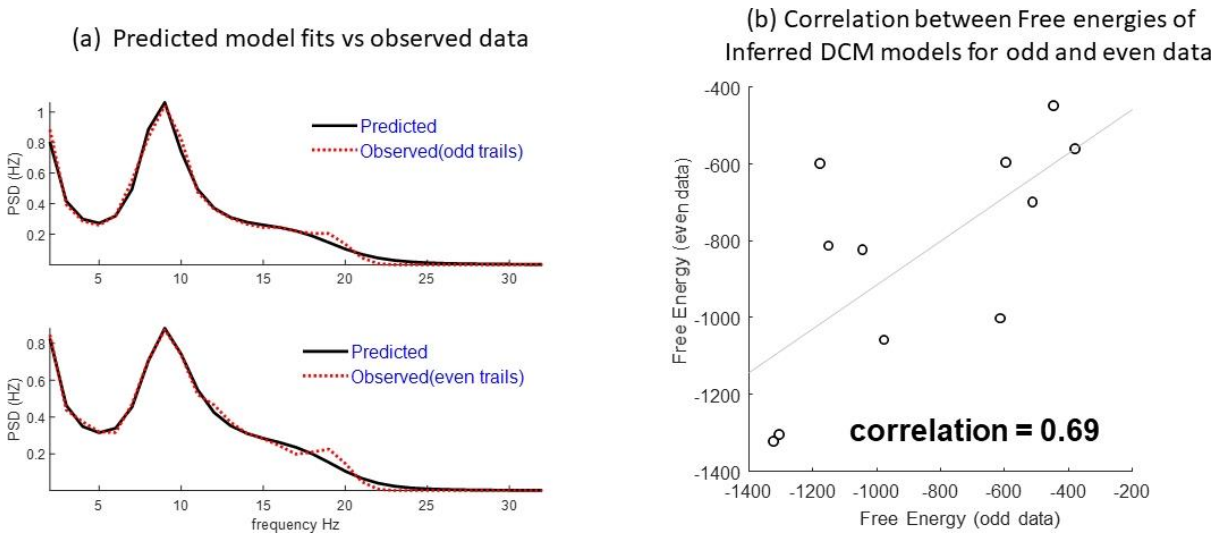

Figure 4. First level DCM results. Panel (a) shows predicted vs observed MEG data for even-Data and odd-Data from a single participant. This panel shows that DCM can explain the spectral dynamics of each dataset well. All inversion results are provided in the supplementary material. Panel (b) shows the correlation between free energies of odd and even datasets over participants (points in the plot). This correlation shows a moderately good level of agreement between the odd-Data and even-Data across all participants.

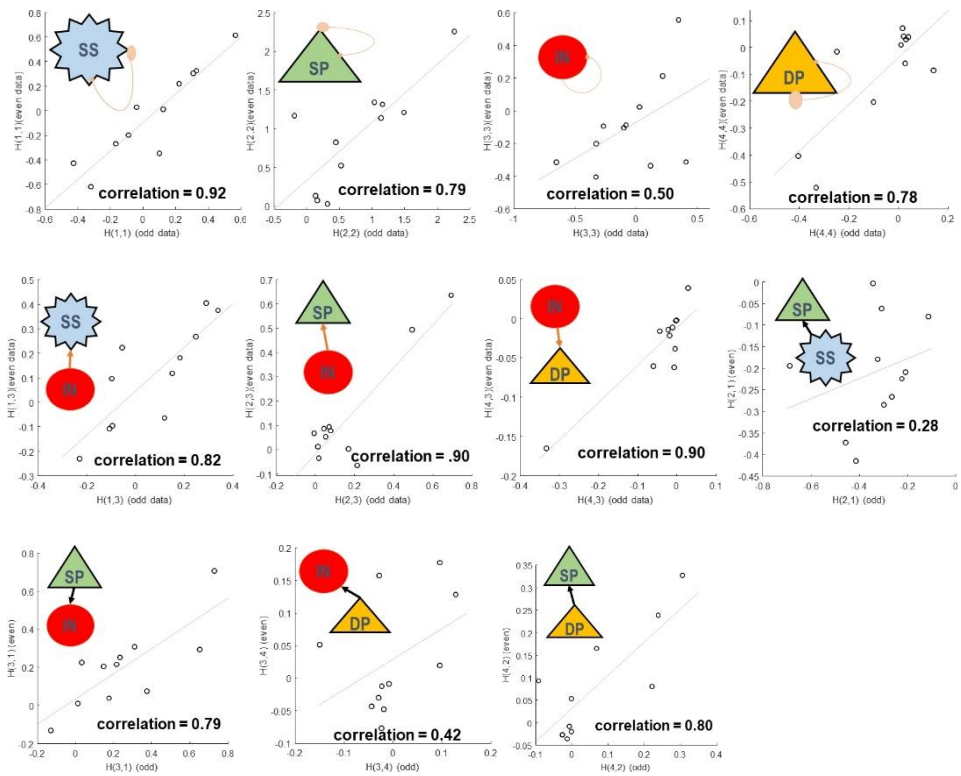

Figure 5. Correlations between inferred synaptic physiology in odd and even epochs. In all figures the inhibitory connections are shown in light orange and excitatory connections are shown in black. $(i,)$ is a connection in the CMM-NMDA model from population j to population i. The spiny stellate population is denoted by ss, the superficial pyramidal cells is denoted by sp, inhibitory interneuron is denoted by in and deep pyramidal cells is denoted by dp. All inferred connections are significantly correlated over subjects, except $dp \rightarrow in$ and $sp \rightarrow ss$.

To confirm the predictive validity of DCM, we calculated the correlation between the inferred synaptic parameters from odd and even PSDs data sets: see Figure 5. Most parameters were estimated reliably (figure 5). There were exceptions, such as the excitatory connections of the deep pyramidal and inhibitory connections and superficial pyramidal cells and inhibitory cells. The low correlation between estimates of some parameters is not surprising for complex nonlinear models with conditional dependencies among parameter estimates (Litvak et al., 2019). It implies that different combinations of synaptic parameters may generate similar physiological data. This means hypotheses may therefore be better tested in terms of model comparison, rather than focus on maximum *a posteriori* parameter estimates of single parameters (Rowe et al., 2010). In the following section, we use the reliable connections—with a correlation of greater than one half—to examine the effect of neurotransmitter concentrations as measured by MRS.

3.2 Associations between synaptic parameters and MRS measures:

The most likely relationship between the synaptic parameters and neurotransmitter levels was identified through the hyperparameter optimization.

3.2.1 MRS-GABA data as an empirical prior on inhibitory synaptic parameters:

MRS GABA was evaluated as an empirical prior constraint on 127 combinations of inhibitory connections (2^7-1, combinations of seven inhibitory connections in the CMM_NMDA model). As each combination might be constrained by empirical MRS-GABA priors, Bayesian model reduction can be used to assess which of the 127 combinations and linear/nonlinear transformations of MRS GABA measures maximise model evidence. Alternatively, one can group certain synaptic parameters based on their common features (self-inhibition vs inter-regional connections or superficial vs deep connections), to identify the winning model 'family' for each subgroup of connections.

We grouped the inhibitory connections into four self-connections and three inter-lamina connections. By grouping the parameters in this way, we ask whether MRS-GABA influences recurrent intra-laminar connectivity, or inhibition between layered populations. We assess the evidence for GABA effects, as mediated through second order polynomial and sigmoid

transformations of the MRS measures. We systematically varied the hyperparameters of the sigmoid function for each subset of self-inhibitory synaptic connections and compared the resulting model evidence.

Figure 6 shows the consistency of the resulting free energy over odd and even epoch datasets. The high reliability suggests that both group inversions converge to the same (global) minima. For each subset of self-inhibitory connections, the sigmoid MRS-GABA hyperpriors maximised the model evidence. The winning models for each subset were then examined to determine which MRS mapping is most likely for each subset of self-inhibitory connections. As shown in Figure 7, priors using a sigmoid transformation of GABA concentration provided the most likely account of intersubject variation in synaptic connectivity; specifically, the recurrent connections or self-inhibition of superficial and deep pyramidal cells.

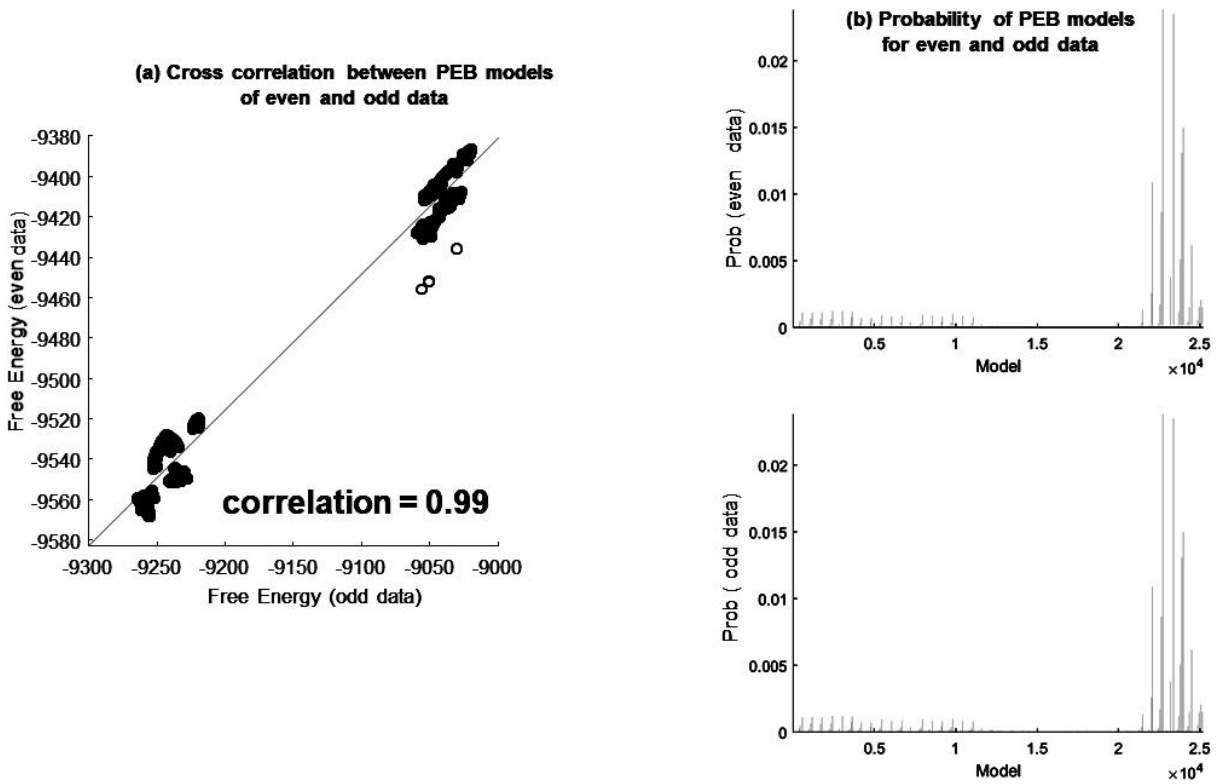

Figure 6. Correlation analysis, comparing the free energy of the PEB model over all subsets of self inhibitory connections and all sigmoid transformations of GABA in odd and even data. This plot shows that the PEB approach consistently estimates the marginal likelihood of models in even and odd data. (b) The probability of different PEB models over model space. Both results show the same maximum. Due to having a large model space, the probability of models and the effect sizes (Free energy) are small (this is known as model dilution).

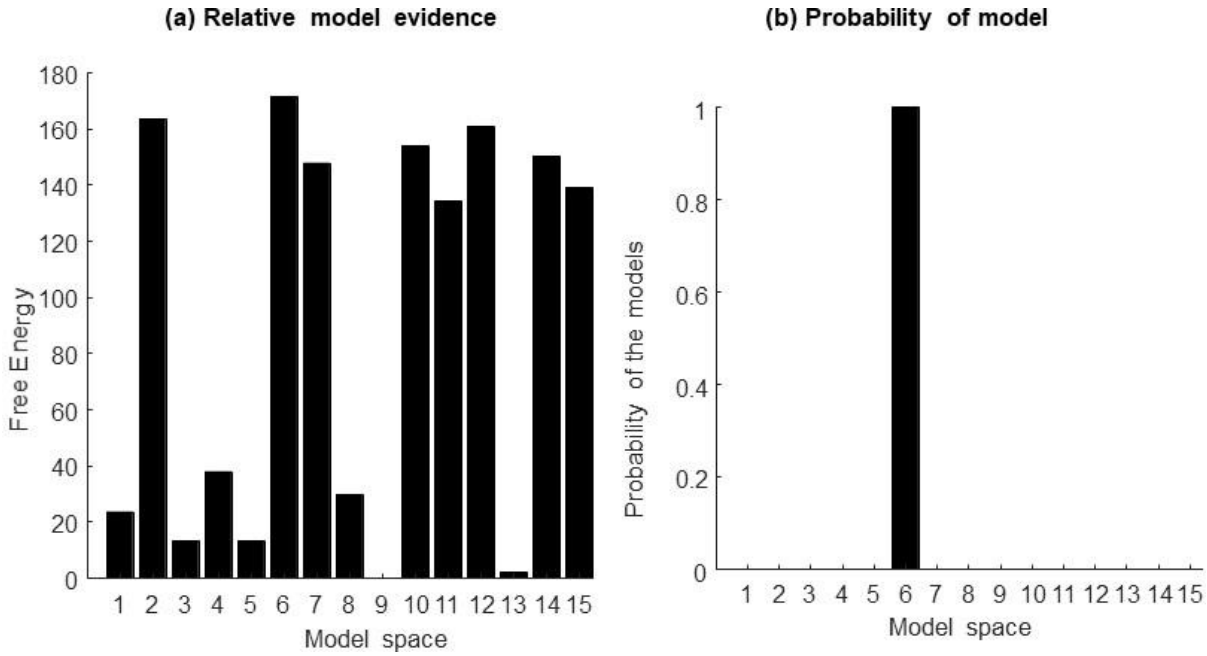

Figure 7. (a) The relative free energy of each subset of the self-inhibitory connections. (b) the probability of each model. The most likely "winning" model is 6 in which a prior of the sigmoid transformation of MRS GABA informs connections H(2,2) and H(4,4).

We repeated the same procedure with inter-laminar (i.e., intrinsic, between population) connections. The results are shown in Figures 8 and 9. MRS GABA provided an informative empirical prior for all inhibitory connections. The MRS transforms for odd and even datasets differ, but are similar in their functional form.

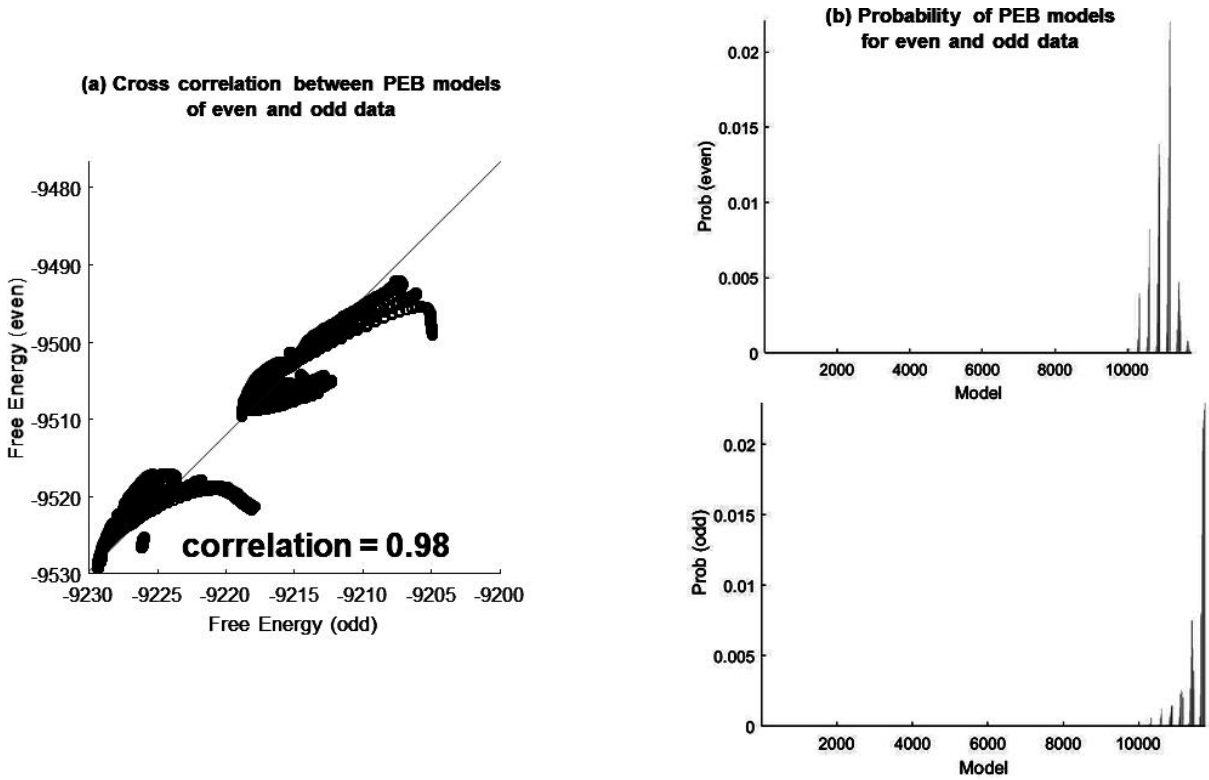

Figure 8. (a) This panel shows a correlation analysis between the free energy from the PEB model that encodes the relationship between all possible inter-regional inhibitory synaptic connections and all possible forms of sigmoid transformation of the MRS-GABA. These results suggests that the PEB approach reliably estimates model evidence in even and odd data. (b) The probability of different PEB models over model space. The maxima in the probability plots are not consistent due to the fact that there are two different MRS transformations with the greatest evidence for the odd and even data. The maximum probability in each plot is associated with the same combination of inhibitory connections.

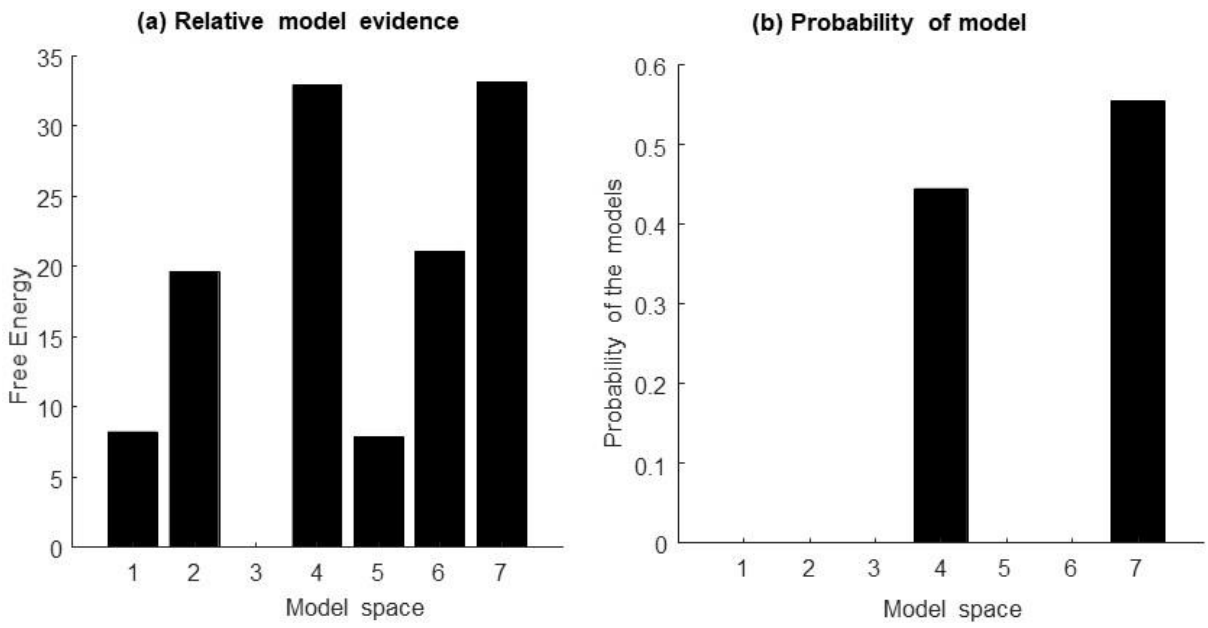

Figure 9. (a) The relative free energy for each subset of inter-laminar inhibitory connections for an optimal transformation is shown(b) The probability of each subset of synaptic connections is illustrated. The winning model identifies connections (2,1) and H(2,4) . In short, a sigmoid transformation of MRS GABA measures the most likely explanation for between subject variation in inhibitory connections H (2,1) and H(2,4) .

We repeated this procedure using a second order polynomial (the first order polynomial is contained within this model space) as the functional form (see supplementary material). We then compared the evidence of the winning models in each analysis; namely, the evidence for the mapping between (sigmoid MRS, self-inhibition), (sigmoid MRS, inter regions), (polynomial MRS, self-inhibition) and (polynomial MRS, inter regions), as shown in Figure 10. The results suggest that the sigmoid transformation is the most likely functional form to explain intersubject variability in the inhibitory recurrent (self) connections in superficial and deep layers.

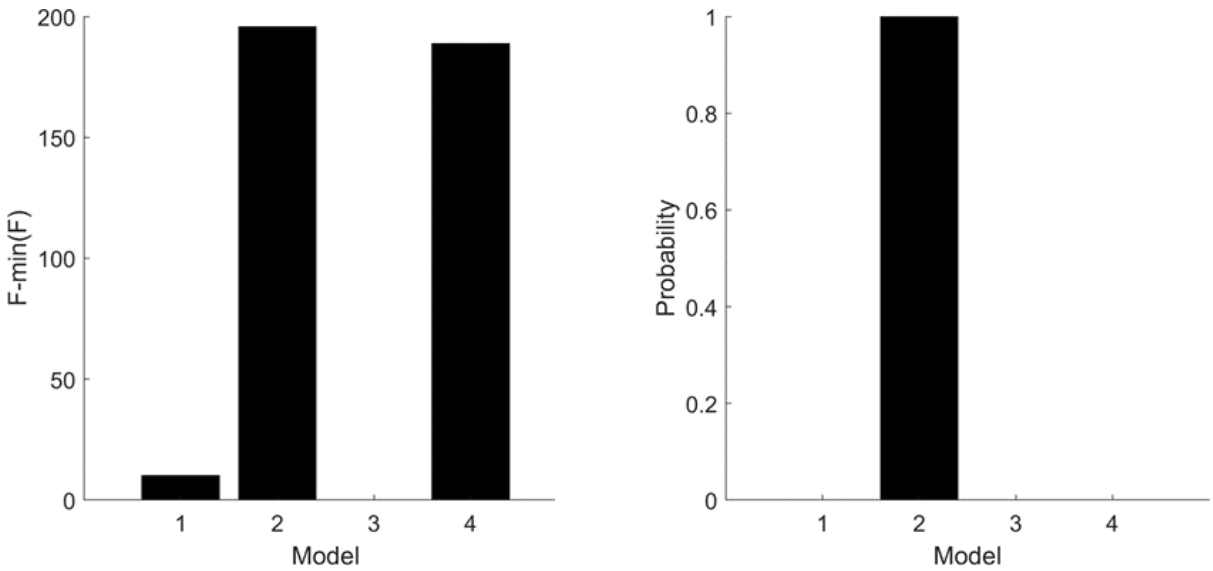

Figure 10. Comparing the probability of sigmoid and second order models that encode the mapping from MRS GABA to self inhibitory connections (model 2, 4) and interlaminar inhibitory connections (model 1 ,3). The comparison indicates the second model is most likely: a sigmoid transformation of MRS GABA informs the recurrent or self-inhibition of deep and superficial populations.

3.2.2 MRS-GLU data as an empirical prior for excitatory synaptic parameters:

We repeated the above analysis to identify the relationship between glutamate (GLU) concentration and excitatory synaptic connections. We considered different combinations of the excitatory connections over sigmoid and second order polynomial functional forms of the relationship between MRS and synaptic parameters. The correlations of models' free energy over odd and even data is shown in Figure 11. The winning model over the complete search space confirms that MRS-GLU is linked to excitatory connections from superficial to deep layers and superficial to inhibitory interneurons (model 3).

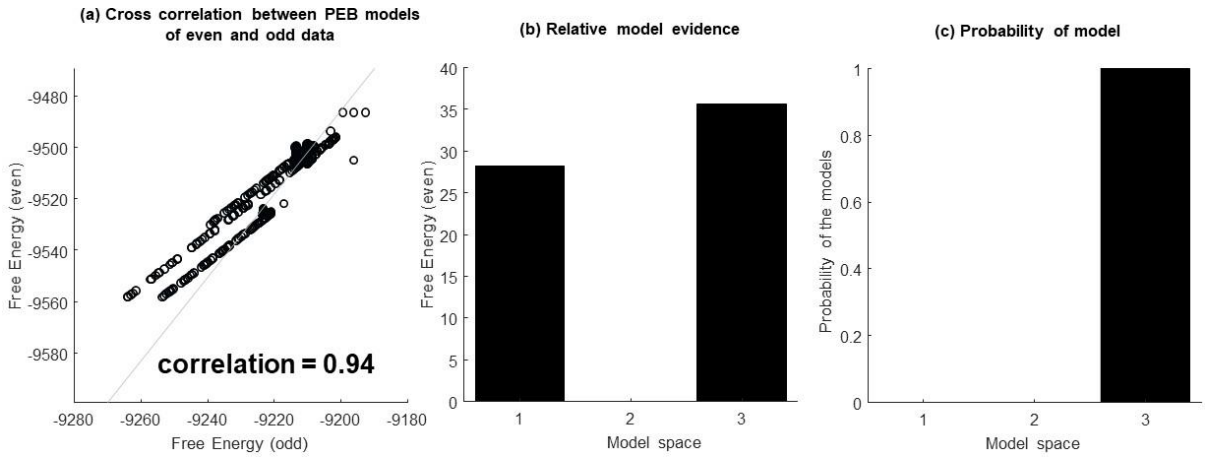

Figure 11. (a) Correlation analysis between the free energy of the PEB model for odd and even data. This plot shows that the PEB approach consistently evaluates model evidence in even and odd data. (b) Free energy and probability of models for the odd and even data are illustrated. Model 1 includes effects on excitatory connections from superficial to deep layers, model 2 considers excitatory connections from superficial excitatory populations to inhibitory interneurons, and model 3 includes both (c) The transformation of the GLU that gives the maximum evidence for the odd and even data. Although, there are two MRS functions that maximise model evidence for the odd and even data, both maps suggest similar nonlinear thresholding of GLU measures provide plausible empirical priors.

The results of comparing a polynomial form and sigmoid transformation of MRS-glutamate measures suggest that a sigmoid transformation is more likely (see Figure 12 and supplementary material).

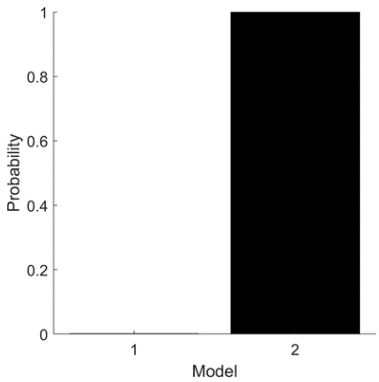

Figure 12. Comparing the probability of models that encode the mapping between MRS GLU measures and excitatory connections (model 1 is a second order polynomial and model 2 corresponds to a sigmoid function). The comparison indicates model 2 is the most likely: a sigmoid transformation of MRS GLU measures informs the excitatory connections between deep and superficial layers.

Discussion:

We present a framework for specifying and comparing hypotheses of the relationship between synaptic physiology and neurotransmitter levels, based on a combination of resting-state magnetoencephalography and magnetic resonance spectroscopy. This enables one to specify and compare the effect of biomarkers of inter-subject variation as informative priors on synaptic parameters in a time efficient and Bayes-optimal manner. The method is applicable to generative models of evoked and resting state time series, recorded by magnetoencephalography, electroencephalography or fMRI. In principle, the individual differences specified here—by MRS—could be replaced by other imaging modalities, or regional neuropathology.

We illustrate how the method can be used to test, non-invasively, hypotheses about the relationship between synaptic physiology and neurotransmitter concentrations in humans. This goes beyond the correlation between M/EEG data features and MRS estimates of neurotransmitter concentration (McColgan et al., 2020), in using formal, generative models of the neurophysiological observations. It is computationally efficient, using first level DCM once and re-evaluating the DCM parameters and model evidence analytically using Bayesian Model Reduction. The model evidence is thereby compared between models with and without the MRS priors, in contrast to the reinversion of the DCMs for alternative priors (Stephan et al., 2009).

We provide evidence that a non-linear transform of the MRS GABA measures offers the best explanation for inter-subject variability in inhibitory recurrent (i.e., self) connectivity of superficial and deep neuronal populations. In addition, a sigmoid transform of the MRS glutamate provides the best explanation of inter-subject variations in excitatory connections from superficial to deep layers. The identification of a sigmoid form for the MRS transform is interesting, because experimental changes of GABA/GLU concentrations exhibit a sigmoid relationship to neuronal responses (their postsynaptic gains) (Benardete and Kriegstein, 2002, Dyke et al., 2017, Chebib et al., 2009). The relationship between superficial and deep layer connectivity is especially relevant to studies of neuropsychiatric and neurological disorders with abnormalities in GABA and glutamate, e.g., schizophrenia, movement disorders and dementia (Adams et al., 2021, Murley et al., 2020, Murley et al., 2022). Using MRS data as an

empirical prior on the synaptic connections may provide valuable information about the impact of neuropathology on synaptic function and the response to treatment.

There are several limitations to this study. We focus on the relationship between neurochemical concentrations and synaptic physiology in one cortical region. The choice of the right inferior frontal gyrus was motivated by our interest in frontal lobe function and its impairment in frontotemporal lobar degeneration (Eliasova et al., 2014, Hughes et al., 2015, Murley et al., 2020, Murley et al., 2022) and other neuropsychiatric disorders. However, the method can be applied to multiple regions. For instance, one could combine neurophysiology and spectroscopy from principal nodes in the default mode or salience networks; and test whether MRS data at different regions are associated with extrinsic (between-source) and intrinsic (within-source) connections. Such an approach could test whether local neurotransmitter concentrations in one source influence the activity and connectivity of other sources.

Our study size was modest, although similar to (Stephan et al., 2009), where a related method for DCM was described. A larger sample size could widen the intersubject distribution, and facilitate the inversion of the hierarchical models (Kerkhoff and Nussbeck, 2019). However, the Bayes factors indicate that our study had sufficient precision (sufficient 'power' by analogy to frequentist testing) to support the inferences made. Although we draw inferences about the role of GABA and glutamate on neurophysiological function, and synaptic connectivity specifically, we do not ,in this study, perturb such functions through psychopharmacological challenges. The combination of the current analysis with GABAergic or glutamatergic interventions could be used to identify baseline dependent effects of drug interventions, as in (Adams et al., 2021) within a simpler and integrated Bayesian modelling procedure.

In conclusion, we propose that dynamic causal models of neurophysiology can be explicitly informed by priors based on measures of individual differences in neurochemistry, molecular pathology or cell/synapse specific loss. The enrichment of DCMs by such markers of inter-subject variability has many potential applications, exploiting the computational efficiencies of parametric empirical Bayesian methods and Bayesian Model Reduction with hierarchical inversion of individual and group-level models of functional imaging data.

Acknowledgements

This work has been funded by the Wellcome Trust (220258), the Medical Research Council (SUAG/092 G116768) and Cambridge Centre for Parkinson-plus; the Holt fellowship; and the NIHR Cambridge Biomedical Research Centre (BRC-1215-20014). KJF is supported by funding for the Wellcome Centre for Human Neuroimaging (Ref: 205103/Z/16/Z) and a Canada-UK Artificial Intelligence Initiative (Ref: ES/T01279X/1). The views expressed are those of the author(s) and not necessarily those of the NIHR or the Department of Health and Social Care. For the purpose of open access, the authors have applied a CC BY public copyright licence to any Author Accepted Manuscript version arising from this submission.

Table:

***Table 1**: Acronyms*

Acronyms	Description
AMPA	α-amino-3-hydroxy-5-methyl-4-isoxazolepropionic acid
BMR	Bayesian model reduction
CMM	Conductance mesoscopic model
DCM	Dynamic causal modelling
FT	Fourier transform
fMRI	Functional magnetic resonance imaging
GABA	Gamma-aminobutyric acid
GLN	Glutamine
GLU	Glutamate
MEG	Magnetoencephalography
MRS	Magnetic resonance spectroscopy
NMDA	N-methyl-D-aspartate receptors
PEB	Parametric empirical Bayes
Odd/Even PSD	Power spectral density that was derived from odd or even trails in MEG data
RIFG	Right inferior frontal gyrus
SP,SS,Inh,DP	Superficial pyramidal cells, spiny stellate excitatory neurons, interneurons, deep pyramidal cells

Table 2: *Glossary of variables and expressions in conductance-based model (CMM)*

Variable	Description
u	Exogenous input
V	Mean depolarisation of a neuronal population
$\sigma(v)$	The neuronal firing rate – a sigmoid squashing function of depolarisation
L	Lead field vector mapping from (neuronal) states to measured (electrophysiological) responses
$g_x(\omega), g_o(\omega), g_y(\omega)$	Spectral density of (neuronal) state fluctuations, observation noise and measurement, respectively
$\nabla_x f$	System Jacobian or derivative of system flow with respect to (neuronal) states
$k(t) = FT[K(\omega)]$	First order kernel mapping from inputs to responses; c.f., an impulse response function of time. This is the Fourier transform of the transfer function
$K(\omega) = FT[k(t)]$	Transfer function of frequency, modulating the power of endogenous neuronal fluctuations to produce a (cross spectral density) response. This is the Fourier transform of the kernel

Table 3*: Parameters of the neuronal model (see also Figure 1)*

	Description	Parameterisation	Prior
τ	Rate constant of ion channels	$exp(\theta_\kappa) \cdot \tau$ $\tau = [256,128,16,32]$	$p(\theta_\kappa) = N(0,1/16)$
C	Membrane capacitance	$exp(\theta_a) \cdot C$	$p(\theta_a) = N(0,1/16)$
H	Intrinsic connections	$exp(\theta_a) \cdot H$ H = $\begin{bmatrix} 8 & 0 & 2 & 0 \\ 4 & 8 & 8 & 0 \\ 0 & 0 & 32 & 128 \end{bmatrix}$	$p(\theta_a) = N(0,1/32)$

***Table4**: Parameterisation of MRS GABA (variable g) and GLU (variable s) transforms.*

Functional description	Parameter range
$\Gamma_\varphi(g) = \frac{1}{1+\exp(-30\exp(\varphi_1)(g-\exp(-5)\exp(\varphi_2)))}$	$\varphi_1 \times \varphi_2 = [-2{:}\,0.1{:}\,2] \times [-1{:}\,0.1{:}\,3]$
$\Gamma_\varphi(g) = \varphi_1 g + \varphi_2\, g^2$	$\varphi_1 \times \varphi_2 = [-10{:}\,.5{:}\,10] \times [-10{:}\,.5{:}\,10]$
$\Gamma_\varphi(s) = \frac{1}{1+\exp(-10\exp(\varphi_1)(s-\exp(-1)\exp(\varphi_2)))}$	$\varphi_1 \times \varphi_2 = [-5{:}\,.1{:}\,5] \times [-4{:}\,.1{:}\,0]$
$\Gamma_\varphi(s) = \varphi_1 s + \varphi_2\, s^2$	$\varphi_1 \times \varphi_2 = [-10{:}\,.5{:}\,10] \times [-10{:}\,.5{:}\,10]$

References:

ADAMS, N., HUGHES, L. E., ROUSE, M. A., PHILLIPS, H. N., SHAW, A. D., MURLEY, A. G., COPE, T., BEVAN-JONES, W. R., PASSAMONTI, L. & HOLLAND, N. 2021. GABAergic cortical network physiology in frontotemporal lobar degeneration.

BASAR, E., FLOHR, H., HAKEN, H. & MANDELL, A. 2012. *Synergetics of the Brain: Proceedings of the International Symposium on Synergetics at Schloß Elmau, Bavaria, May 2–7, 1983*, Springer Science & Business Media.

BENARDETE, E. A. & KRIEGSTEIN, A. R. 2002. Increased excitability and decreased sensitivity to GABA in an animal model of dysplastic cortex. *Epilepsia,* 43**,** 970-982.

BISHOP, C. M. 2006. *Pattern recognition and machine learning*, springer.

BLÜML, S. & PANIGRAHY, A. 2012. *MR spectroscopy of pediatric brain disorders*, Springer Science & Business Media.

BOUMEZBEUR, F., MASON, G. F., DE GRAAF, R. A., BEHAR, K. L., CLINE, G. W., SHULMAN, G. I., ROTHMAN, D. L. & PETERSEN, K. F. 2010. Altered brain mitochondrial metabolism in healthy aging as assessed by in vivo magnetic resonance spectroscopy. *Journal of Cerebral Blood Flow & Metabolism,* 30**,** 211-221.

CHEBIB, M., GAVANDE, N., WONG, K. Y., PARK, A., PREMOLI, I., MEWETT, K. N., ALLAN, R. D., DUKE, R. K., JOHNSTON, G. A. & HANRAHAN, J. R. 2009. Guanidino acids act as ρ1 GABA C receptor antagonists. *Neurochemical research,* 34**,** 1704-1711.

CHOWDHURY, G. M., BEHAR, K. L., CHO, W., THOMAS, M. A., ROTHMAN, D. L. & SANACORA, G. 2012. 1H-[13C]-nuclear magnetic resonance spectroscopy measures of ketamine's effect on amino acid neurotransmitter metabolism. *Biological psychiatry,* 71**,** 1022-1025.

COHEN, S. M., TSIEN, R. W., GOFF, D. C. & HALASSA, M. M. 2015. The impact of NMDA receptor hypofunction on GABAergic neurons in the pathophysiology of schizophrenia. *Schizophrenia research,* 167**,** 98-107.

DEELCHAND, D. K., ADANYEGUH, I. M., EMIR, U. E., NGUYEN, T. M., VALABREGUE, R., HENRY, P. G., MOCHEL, F. & ÖZ, G. 2015. Two-site reproducibility of cerebellar and brainstem neurochemical profiles with short-echo, single-voxel MRS at 3T. *Magnetic resonance in medicine,* 73**,** 1718-1725.

DUARTE, J. M. & XIN, L. 2019. Magnetic resonance spectroscopy in schizophrenia: evidence for glutamatergic dysfunction and impaired energy metabolism. *Neurochemical research,* 44**,** 102-116.

DYKE, K., PÉPÉS, S. E., CHEN, C., KIM, S., SIGURDSSON, H. P., DRAPER, A., HUSAIN, M., NACHEV, P., GOWLAND, P. A. & MORRIS, P. G. 2017. Comparing GABA-dependent physiological measures of inhibition with proton magnetic resonance spectroscopy measurement of GABA using ultra-high-field MRI. *Neuroimage,* 152**,** 360-370.

ELIASOVA, I., ANDERKOVA, L., MARECEK, R. & REKTOROVA, I. 2014. Non-invasive brain stimulation of the right inferior frontal gyrus may improve attention in early Alzheimer's disease: a pilot study. *Journal of the neurological sciences,* 346**,** 318-322.

FRISTON, K., MATTOUT, J., TRUJILLO-BARRETO, N., ASHBURNER, J. & PENNY, W. 2007. Variational free energy and the Laplace approximation. *Neuroimage,* 34**,** 220-234.

FRISTON, K., PARR, T. & ZEIDMAN, P. 2018. Bayesian model reduction. *arXiv preprint arXiv:1805.07092*.

FRISTON, K. & PENNY, W. 2011. Post hoc Bayesian model selection. *Neuroimage,* 56**,** 2089-2099.

FRISTON, K., ZEIDMAN, P. & LITVAK, V. 2015. Empirical Bayes for DCM: a group inversion scheme. *Frontiers in systems neuroscience,* 9**,** 164.

FRISTON, K. J. 2011. Functional and effective connectivity: a review. *Brain connectivity,* 1**,** 13-36.

FRISTON, K. J., BASTOS, A., LITVAK, V., STEPHAN, K. E., FRIES, P. & MORAN, R. J. 2012. DCM for complex-valued data: cross-spectra, coherence and phase-delays. *Neuroimage,* 59**,** 439-455.

FRISTON, K. J., HARRISON, L. & PENNY, W. 2003. Dynamic causal modelling. *Neuroimage,* 19**,** 1273-1302.

FRISTON, K. J., LI, B., DAUNIZEAU, J. & STEPHAN, K. E. 2011. Network discovery with DCM. *Neuroimage,* 56**,** 1202-1221.

FRISTON, K. J., LITVAK, V., OSWAL, A., RAZI, A., STEPHAN, K. E., VAN WIJK, B. C., ZIEGLER, G. & ZEIDMAN, P. 2016. Bayesian model reduction and empirical Bayes for group (DCM) studies. *Neuroimage,* 128**,** 413-431.

FRISTON, K. J., PRELLER, K. H., MATHYS, C., CAGNAN, H., HEINZLE, J., RAZI, A. & ZEIDMAN, P. 2019. Dynamic causal modelling revisited. *Neuroimage,* 199**,** 730-744.

FRISTON, K. J., TRUJILLO-BARRETO, N. & DAUNIZEAU, J. 2008. DEM: a variational treatment of dynamic systems. *Neuroimage,* 41**,** 849-885.

GAWNE, T. J., OVERBEEK, G. J., KILLEN, J. F., REID, M. A., KRAGULJAC, N. V., DENNEY, T. S., ELLIS, C. A. & LAHTI, A. C. 2020. A multimodal magnetoencephalography 7 T fMRI and 7 T proton MR spectroscopy study in first episode psychosis. *npj Schizophrenia,* 6**,** 1-9.

GREENHOUSE, I., KING, M., NOAH, S., MADDOCK, R. J. & IVRY, R. B. 2017. Individual differences in resting corticospinal excitability are correlated with reaction time and GABA content in motor cortex. *Journal of Neuroscience,* 37**,** 2686-2696.

GRUETTER, R., SEAQUIST, E. R. & UGURBIL, K. 2001. A mathematical model of compartmentalized neurotransmitter metabolism in the human brain. *American Journal of Physiology-Endocrinology And Metabolism,* 281**,** E100-E112.

GRUETTER, R. & TKÁČ, I. 2000. Field mapping without reference scan using asymmetric echo-planar techniques. *Magnetic Resonance in Medicine: An Official Journal of the International Society for Magnetic Resonance in Medicine,* 43**,** 319-323.

HAKEN, H. 1977. Synergetics. *Physics Bulletin,* 28**,** 412.

HUGHES, L. E., RITTMAN, T., REGENTHAL, R., ROBBINS, T. W. & ROWE, J. B. 2015. Improving response inhibition systems in frontotemporal dementia with citalopram. *Brain,* 138**,** 1961-1975.

JAFARIAN, A., ZEIDMAN, P., LITVAK, V. & FRISTON, K. 2019. Structure learning in coupled dynamical systems and dynamic causal modelling. *Philosophical Transactions of the Royal Society A,* 377**,** 20190048.

JELEN, L. A., KING, S., MULLINS, P. G. & STONE, J. M. 2018. Beyond static measures: A review of functional magnetic resonance spectroscopy and its potential to investigate dynamic glutamatergic abnormalities in schizophrenia. *Journal of Psychopharmacology,* 32**,** 497-508.

KASS, R. E. & RAFTERY, A. E. 1995. Bayes factors. *Journal of the american statistical association,* 90**,** 773-795.

KOBER, H., NIMSKY, C., MÖLLER, M., HASTREITER, P., FAHLBUSCH, R. & GANSLANDT, O. 2001. Correlation of sensorimotor activation with functional magnetic resonance imaging and magnetoencephalography in presurgical functional imaging: a spatial analysis. *Neuroimage,* 14**,** 1214-1228.

LALLY, N., MULLINS, P. G., ROBERTS, M. V., PRICE, D., GRUBER, T. & HAENSCHEL, C. 2014. Glutamatergic correlates of gamma-band oscillatory activity during cognition: a concurrent ER-MRS and EEG study. *Neuroimage,* 85**,** 823-833.

LIMONGI, R., JEON, P., THEBERGE, J. & PALANIYAPPAN, L. 2021. Counteracting Effect of Glutathione on the Glutamate-Driven Excitation/Inhibition Imbalance in First-Episode Schizophrenia: A 7T Mrs and Dynamic Causal Modeling Study. *Biological Psychiatry,* 89**,** S282.

LITVAK, V., GARRIDO, M., ZEIDMAN, P. & FRISTON, K. 2015. Empirical Bayes for group (DCM) studies: a reproducibility study. *Frontiers in human neuroscience,* 9**,** 670.

LITVAK, V., JAFARIAN, A., ZEIDMAN, P., TIBON, R., HENSON, R. N. & FRISTON, K. There's no such thing as a 'true'model: the challenge of assessing face validity. 2019 IEEE International Conference on Systems, Man and Cybernetics (SMC), 2019. IEEE, 4403-4408.

LITVAK, V., MATTOUT, J., KIEBEL, S., PHILLIPS, C., HENSON, R., KILNER, J., BARNES, G., OOSTENVELD, R., DAUNIZEAU, J. & FLANDIN, G. 2011. EEG and MEG data analysis in SPM8. *Computational intelligence and neuroscience,* 2011.

MCCOLGAN, P., JOUBERT, J., TABRIZI, S. J. & REES, G. 2020. The human motor cortex microcircuit: insights for neurodegenerative disease. *Nature Reviews Neuroscience,* 21**,** 401-415.

MORAN, R. 2015. Deep brain stimulation for neurodegenerative disease: A computational blueprint using dynamic causal modeling. *Progress in Brain Research.* Elsevier.

MORAN, R. J., KIEBEL, S. J., STEPHAN, K. E., REILLY, R., DAUNIZEAU, J. & FRISTON, K. J. 2007. A neural mass model of spectral responses in electrophysiology. *NeuroImage,* 37**,** 706-720.

MORAN, R. J., PINOTSIS, D. A. & FRISTON, K. J. 2013. Neural masses and fields in dynamic causal modeling. *Frontiers in computational neuroscience,* 7**,** 57.

MORAN, R. J., STEPHAN, K. E., DOLAN, R. J. & FRISTON, K. J. 2011. Consistent spectral predictors for dynamic causal models of steady-state responses. *Neuroimage,* 55**,** 1694-1708.

MURLEY, A. G., ROUSE, M. A., JONES, P. S., YE, R., HEZEMANS, F. H., O'CALLAGHAN, C., FRANGOU, P., KOURTZI, Z., RUA, C. & CARPENTER, T. A. 2020. GABA and glutamate deficits from frontotemporal lobar degeneration are associated with disinhibition. *Brain,* 143**,** 3449-3462.

MURLEY, A. G., TSVETANOV, K. A., ROUSE, M. A., JONES, P. S., SVAERKE, K., CARPENTER, T. A. & ROWE, J. B. 2022. Proton magnetic resonance spectroscopy in frontotemporal lobar degeneration-related syndromes. *Neurobiology of Aging,* 111**,** 64-70.

MYERS, J. F., EVANS, C. J., KALK, N. J., EDDEN, R. A. & LINGFORD-HUGHES, A. R. 2014. Measurement of GABA using J-difference edited 1H-MRS following modulation of synaptic GABA concentration with tiagabine. *Synapse,* 68**,** 355-362.

OOSTENVELD, R., FRIES, P., MARIS, E. & SCHOFFELEN, J.-M. 2011. FieldTrip: open source software for advanced analysis of MEG, EEG, and invasive electrophysiological data. *Computational intelligence and neuroscience,* 2011.

PELLERIN, L., BOUZIER-SORE, A. K., AUBERT, A., SERRES, S., MERLE, M., COSTALAT, R. & MAGISTRETTI, P. J. 2007. Activity-dependent regulation of energy metabolism by astrocytes: an update. *Glia,* 55**,** 1251-1262.

RAMAN, S., DESERNO, L., SCHLAGENHAUF, F. & STEPHAN, K. E. 2016. A hierarchical model for integrating unsupervised generative embedding and empirical Bayes. *Journal of neuroscience methods,* 269**,** 6-20.

RIDEAUX, R. 2020. Temporal dynamics of GABA and Glx in the visual cortex. *Eneuro,* 7.

RIDEAUX, R. 2021. No balance between glutamate+ glutamine and GABA+ in visual or motor cortices of the human brain: A magnetic resonance spectroscopy study. *NeuroImage,* 237**,** 118191.

ROWE, J. B., HUGHES, L. E., BARKER, R. A. & OWEN, A. M. 2010. Dynamic causal modelling of effective connectivity from fMRI: are results reproducible and sensitive to Parkinson's disease and its treatment? *Neuroimage,* 52**,** 1015-1026.

SCHMITZ, T. W., CORREIA, M. M., FERREIRA, C. S., PRESCOT, A. P. & ANDERSON, M. C. 2017. Hippocampal GABA enables inhibitory control over unwanted thoughts. *Nature communications,* 8**,** 1-12.

SHAW, A., MORAN, R. J., MUTHUKUMARASWAMY, S. D., BREALY, J., LINDEN, D., FRISTON, K. J. & SINGH, K. D. 2017. Neurophysiologically-informed markers of individual variability and pharmacological manipulation of human cortical gamma. *Neuroimage,* 161**,** 19-31.

SOKOLOV, A. A., ZEIDMAN, P., ERB, M., RYVLIN, P., PAVLOVA, M. A. & FRISTON, K. J. 2019. Linking structural and effective brain connectivity: structurally informed Parametric Empirical Bayes (si-PEB). *Brain structure & function,* 224**,** 205-217.

SPIVAK, M. 2020. *Calculus: càlcul infinitesimal*, Reverté.

STAGG, C., BESTMANN, S., CONSTANTINESCU, A., MORENO MORENO, L., ALLMAN, C., MEKLE, R., WOOLRICH, M., NEAR, J., JOHANSEN-BERG, H. & ROTHWELL, J. 2011. Relationship between physiological measures of excitability and levels of glutamate and GABA in the human motor cortex. *The Journal of physiology,* 589**,** 5845-5855.

STAGG, C. & ROTHMAN, D. 2013. *Magnetic resonance spectroscopy: tools for neuroscience research and emerging clinical applications*, Academic Press.

STEEL, A., MIKKELSEN, M., EDDEN, R. A. & ROBERTSON, C. E. 2020. Regional balance between glutamate+ glutamine and GABA+ in the resting human brain. *Neuroimage,* 220**,** 117112.

STEFANOVSKI, L., TRIEBKORN, P., SPIEGLER, A., DIAZ-CORTES, M.-A., SOLODKIN, A., JIRSA, V., MCINTOSH, A. R., RITTER, P. & INITIATIVE, A. S. D. N. 2019. Linking molecular pathways and large-scale computational modeling to assess candidate disease mechanisms and pharmacodynamics in Alzheimer's disease. *Frontiers in computational neuroscience,* 13**,** 54.

STEPHAN, K. E., TITTGEMEYER, M., KNÖSCHE, T. R., MORAN, R. J. & FRISTON, K. J. 2009. Tractography-based priors for dynamic causal models. *Neuroimage,* 47**,** 1628-1638.

VAN DER GRAAF, M. 2010. In vivo magnetic resonance spectroscopy: basic methodology and clinical applications. *European Biophysics Journal,* 39**,** 527-540.

WANG, H., TAN, L., WANG, H.-F., LIU, Y., YIN, R.-H., WANG, W.-Y., CHANG, X.-L., JIANG, T. & YU, J.-T. 2015. Magnetic resonance spectroscopy in Alzheimer’s disease: systematic review and meta-analysis. *Journal of Alzheimer's Disease,* 46**,** 1049-1070.

ZEIDMAN, P., JAFARIAN, A., CORBIN, N., SEGHIER, M. L., RAZI, A., PRICE, C. J. & FRISTON, K. J. 2019a. A guide to group effective connectivity analysis, part 1: First level analysis with DCM for fMRI. *NeuroImage,* 200**,** 174-190.

ZEIDMAN, P., JAFARIAN, A., SEGHIER, M. L., LITVAK, V., CAGNAN, H., PRICE, C. J. & FRISTON, K. J. 2019b. A guide to group effective connectivity analysis, part 2: Second level analysis with PEB. *NeuroImage,* 200**,** 12-25.

4 Supplementary figures

Figure 13 shows the first level DCM results across all eleven participant. Figure 14 illustrate model comparison of second level PEB associated with self-inhibitory connections (top) and inter-regional connections (bottom plot) given class of first and second order polynomial maps for MRS data as their regressors.

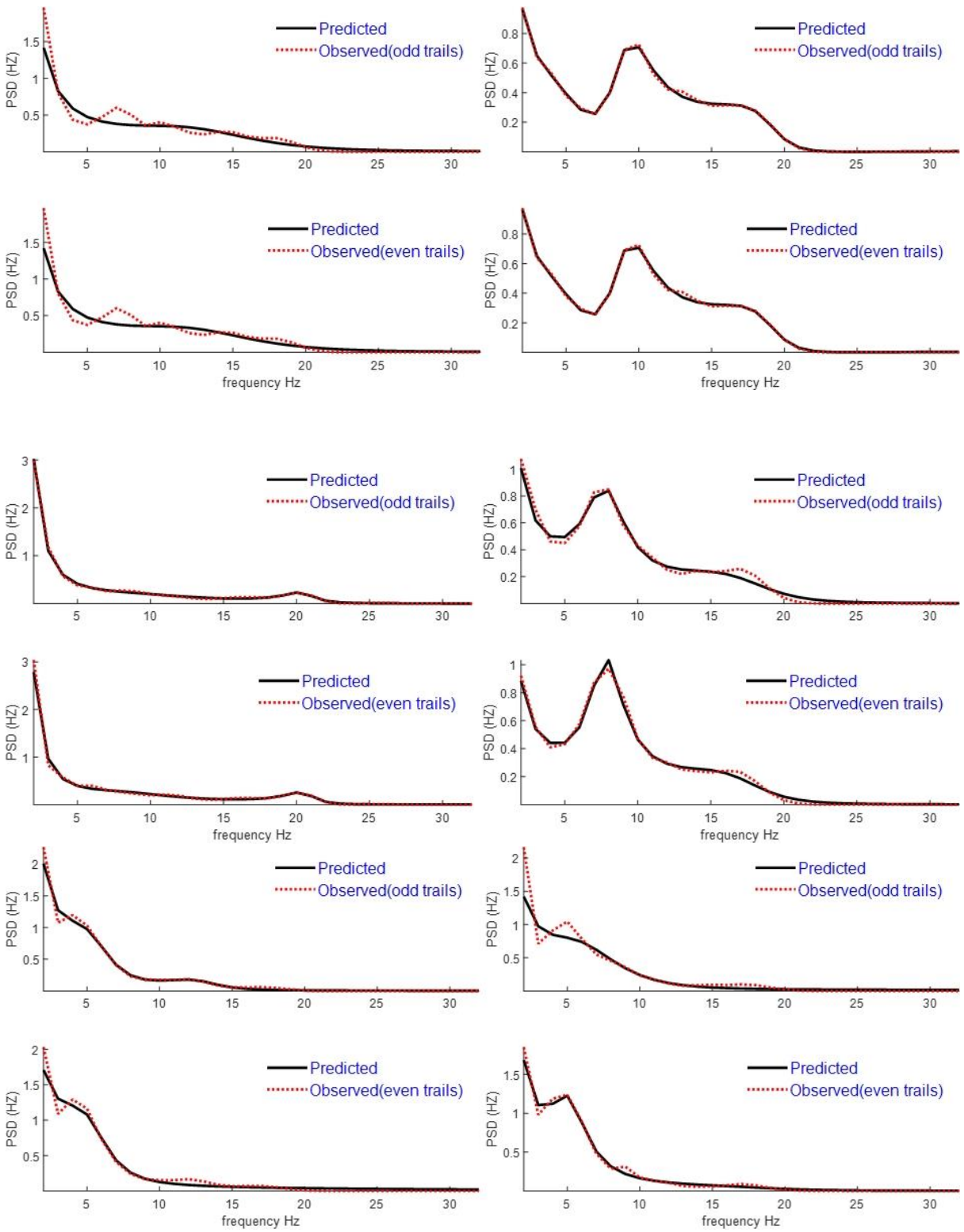
Predicted
Observed(odd trails)
Observed(even trails)
PSD (HZ)
frequency Hz

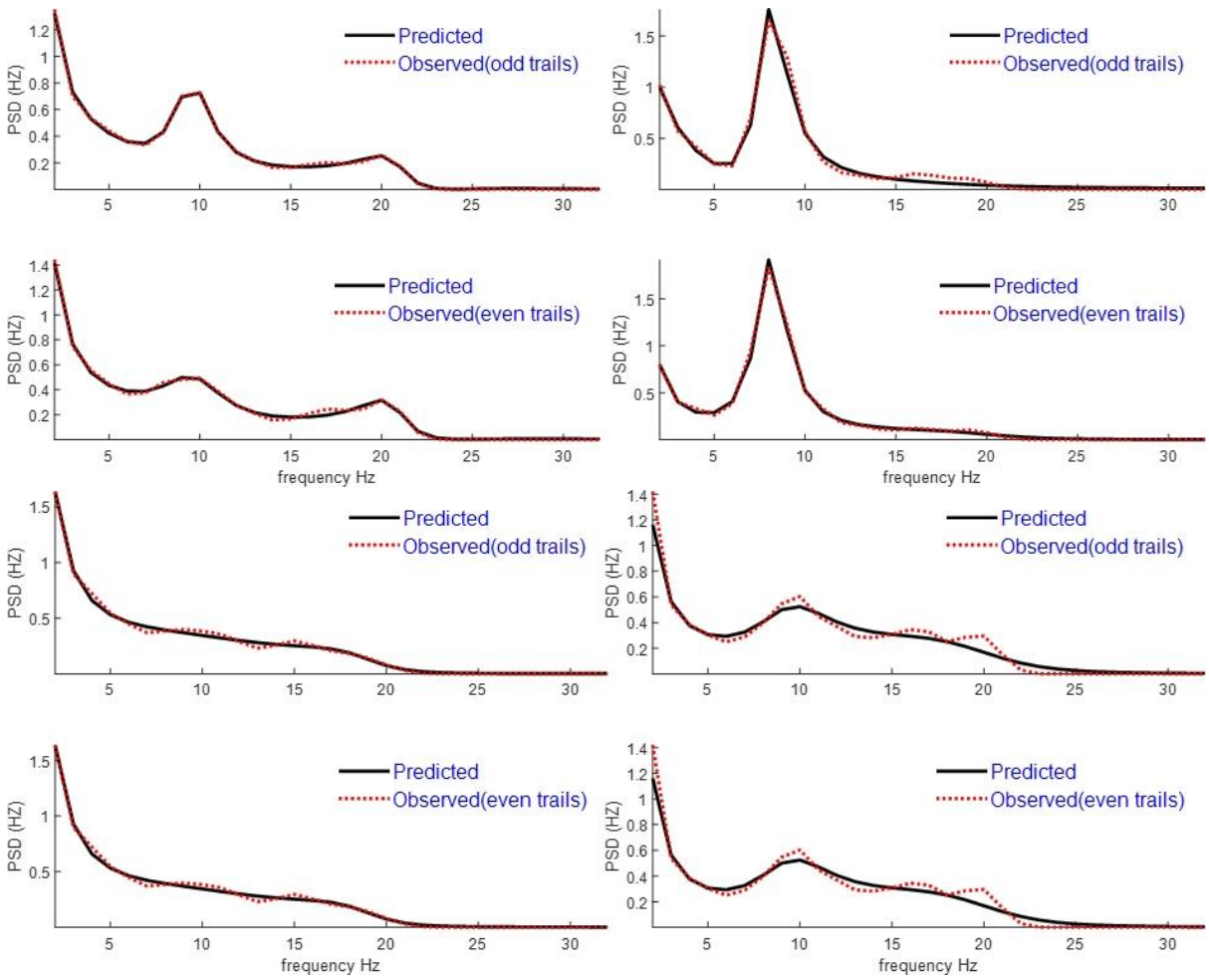

Figure 13. First level DCM predicted vs observed data for each subject even and odd PSD data.

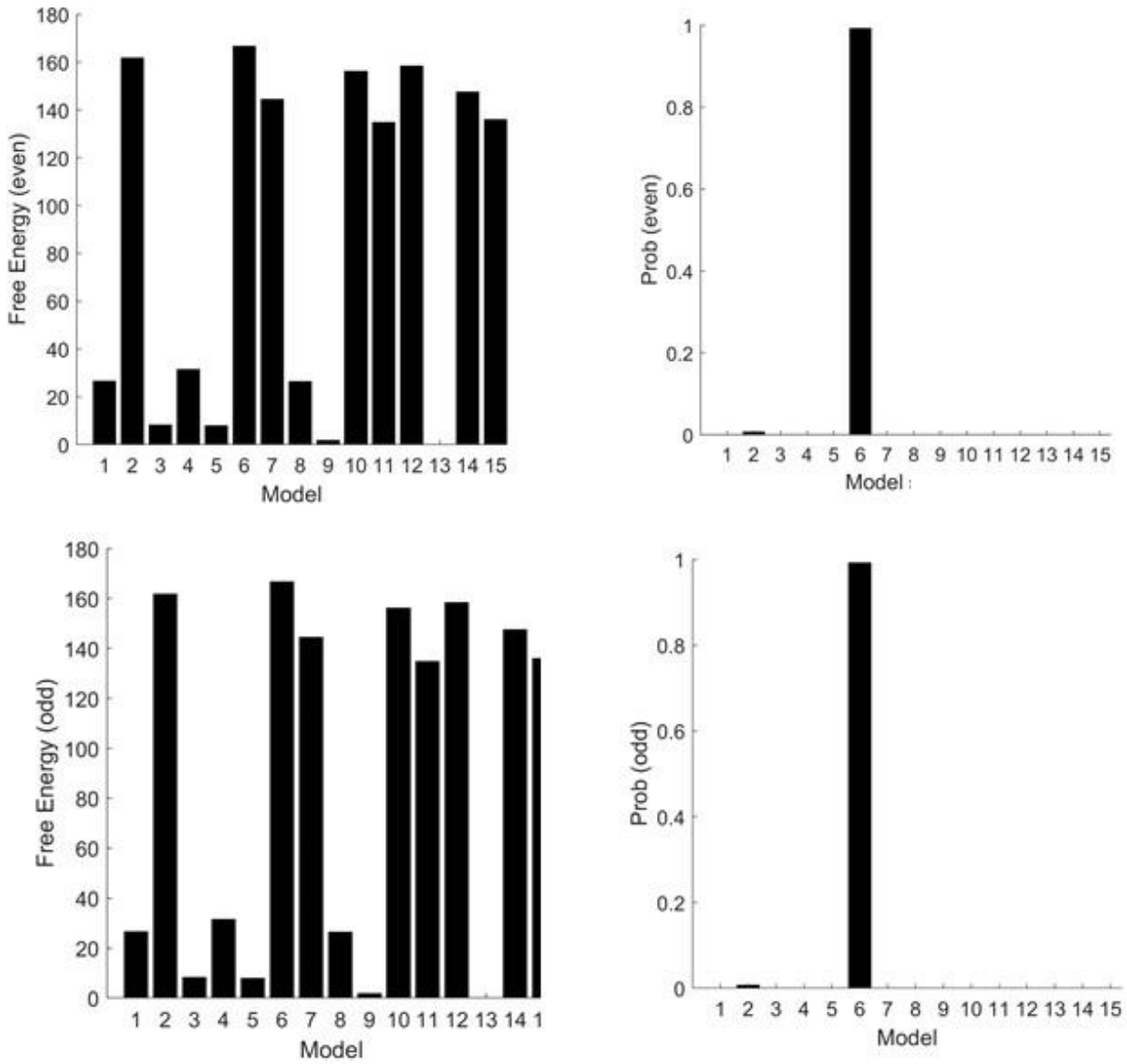
Free Energy (even)
Model
Prob (even)
Model
Free Energy (odd)
Model
Prob (odd)
Model

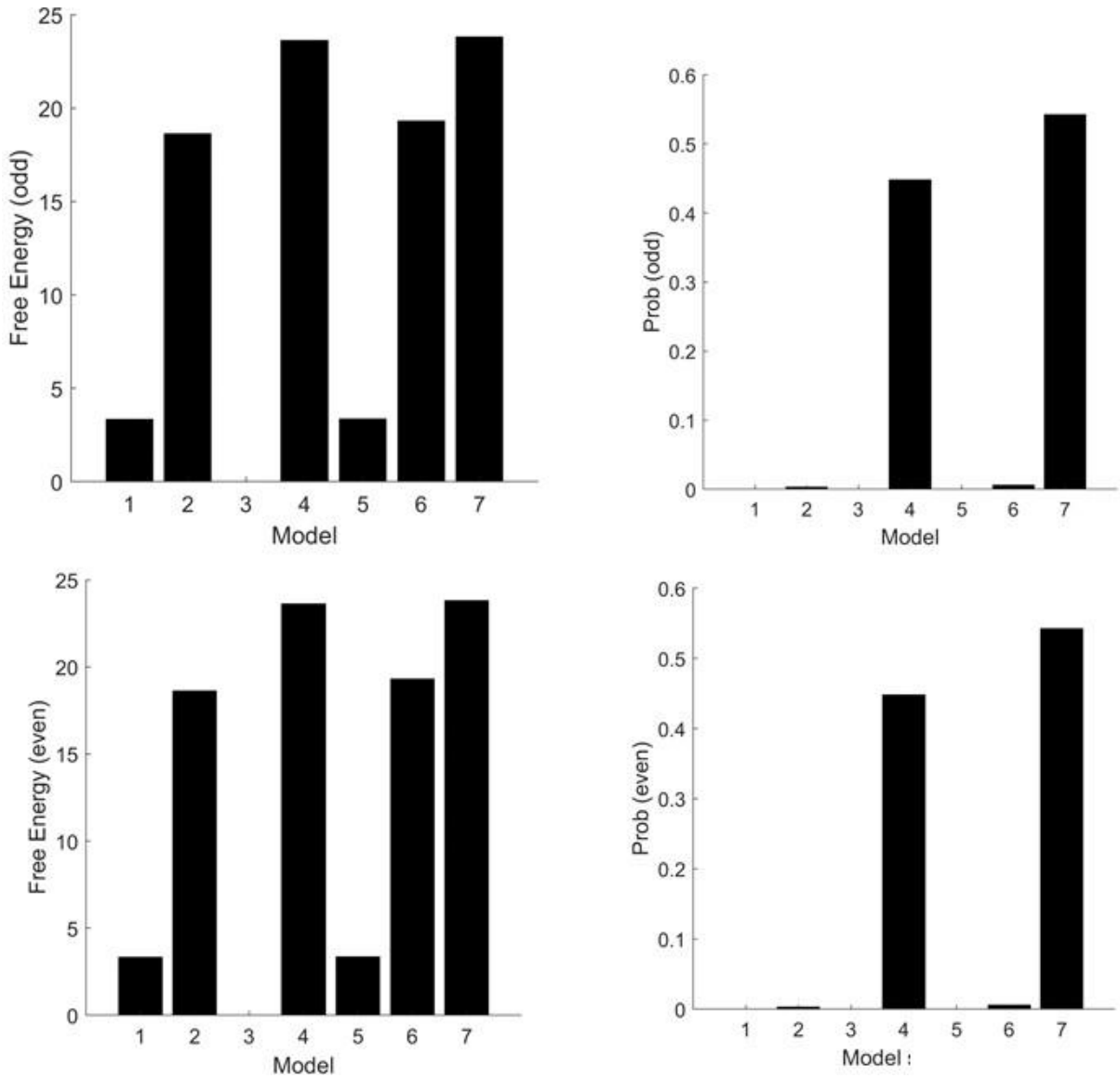

Figure 14 The following figures shows the second level PEB model comparison results with MRS maps (class of first and second order polynomial) as their regressors. . The model comparison associated with different combinations of self-inhibitory connections are at top plot and the model comparison associated with different combinations of inter-regional connections are at the bottom plot.

Supplementary figures : Neurochemistry-enriched dynamic causal models of magnetoencephalography, using magnetic resonance spectroscopy

Amirhossein Jafarian[1], Laura Hughes[1,2], Natalie E Adams[1], Juliette Lanskey[2], Michelle Naessens[1], Matthew A Rouse[1,2] , Alexander G Murley[1], Karl J Friston[3], James B Rowe[1,2]

[1] Department of Clinical Neurosciences and Cambridge University Hospitals NHS Trust, University of Cambridge, United Kingdom

[2] MRC Cognition and Brain Sciences Unit, University of Cambridge, Cambridge, UK

[3] The Wellcome Centre for Human Neuroimaging, UCL Queen Square Institute of Neurology, United Kingdom

Figure 13 shows the first level DCM results across all eleven participant. Figure 14 illustrate model comparison of second level PEB associated with self-inhibitory connections (top) and inter-regional connections (bottom plot) given class of first and second order polynomial maps for MRS data as their regressors.

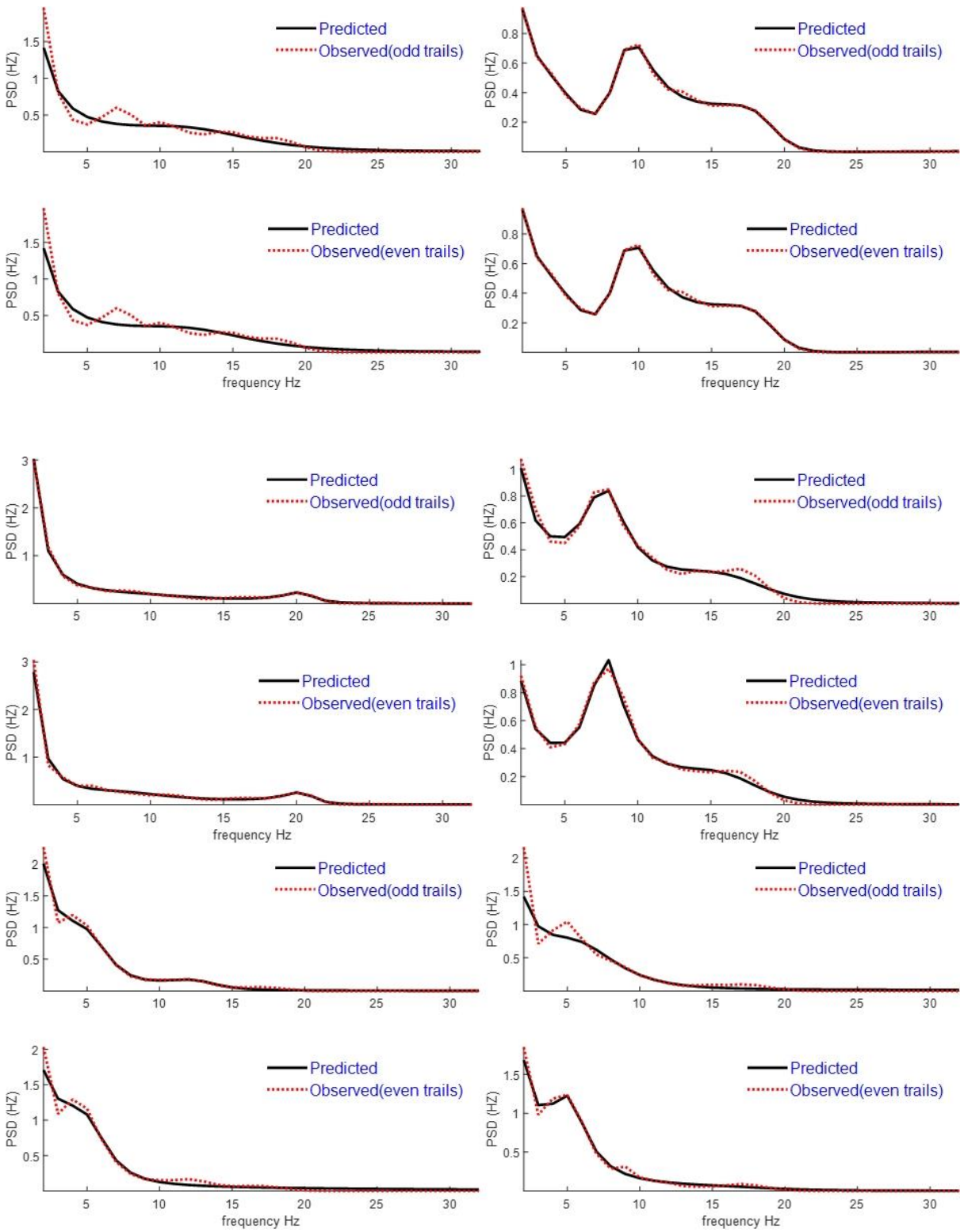
Predicted
Observed(odd trails)
Observed(even trails)
PSD (HZ)
frequency Hz

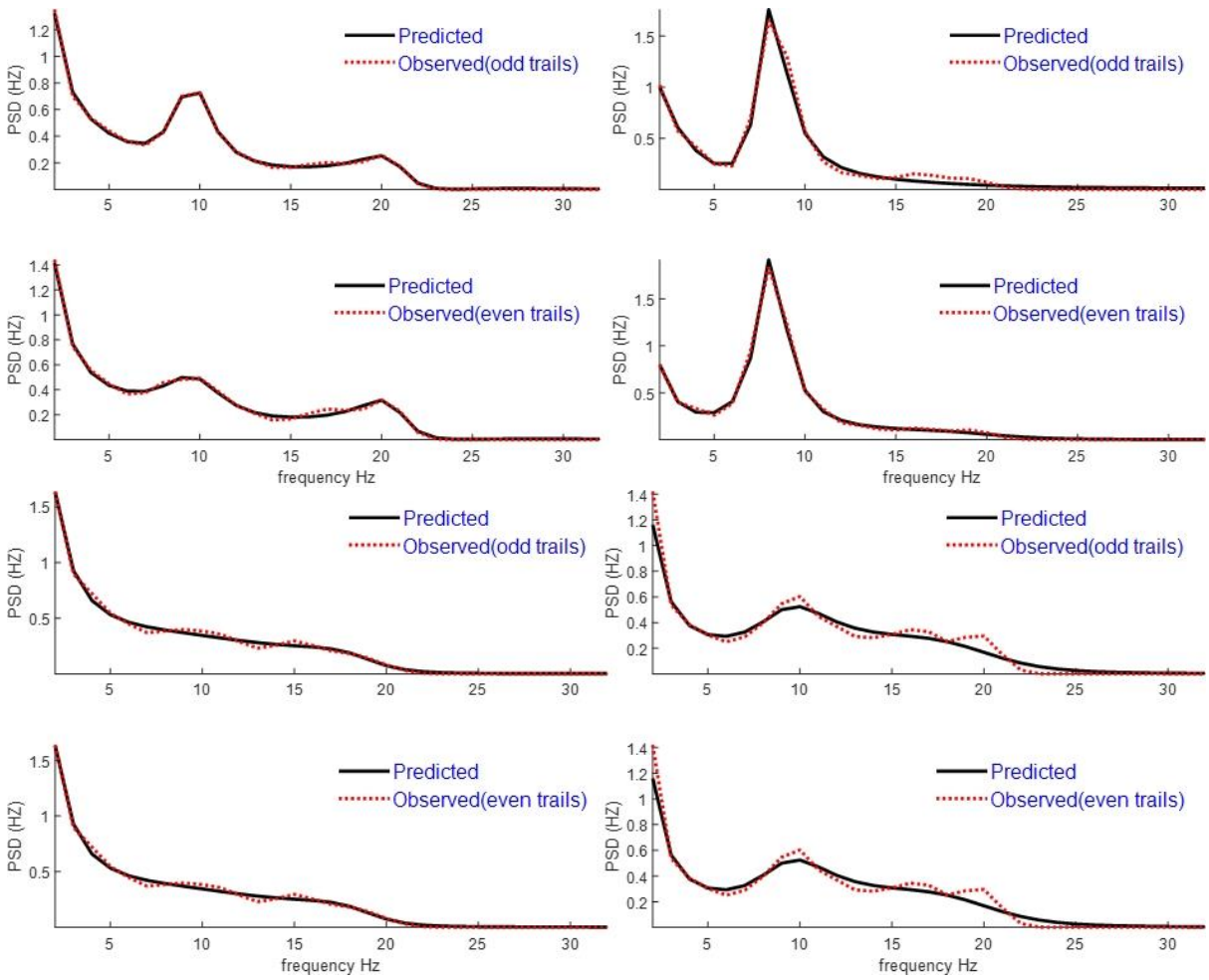

Figure 1. First level DCM predicted vs observed data for both even and odd PSD for each subject.

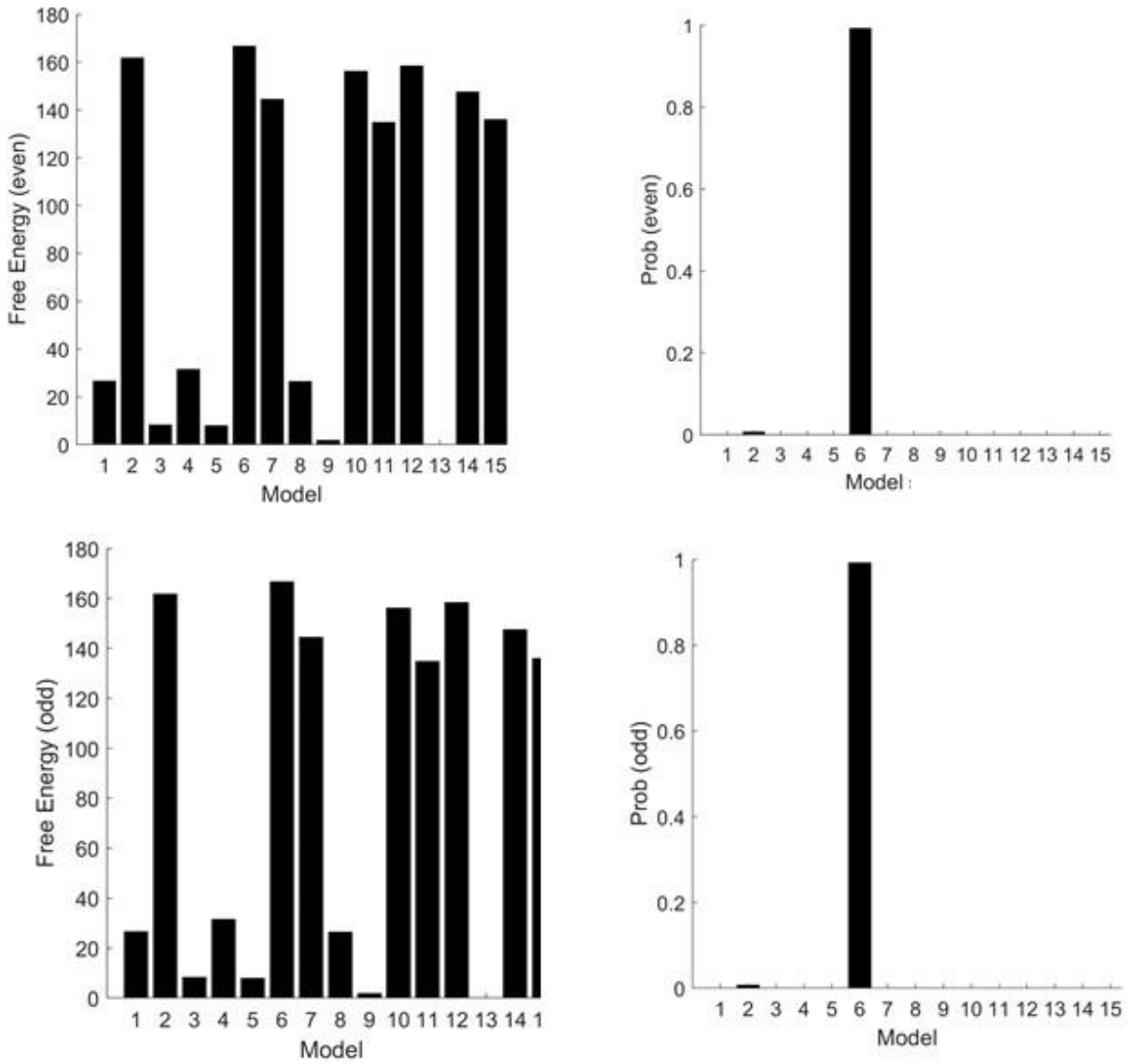
Free Energy (even)
Model
Prob (even)
Model
Free Energy (odd)
Model
Prob (odd)
Model

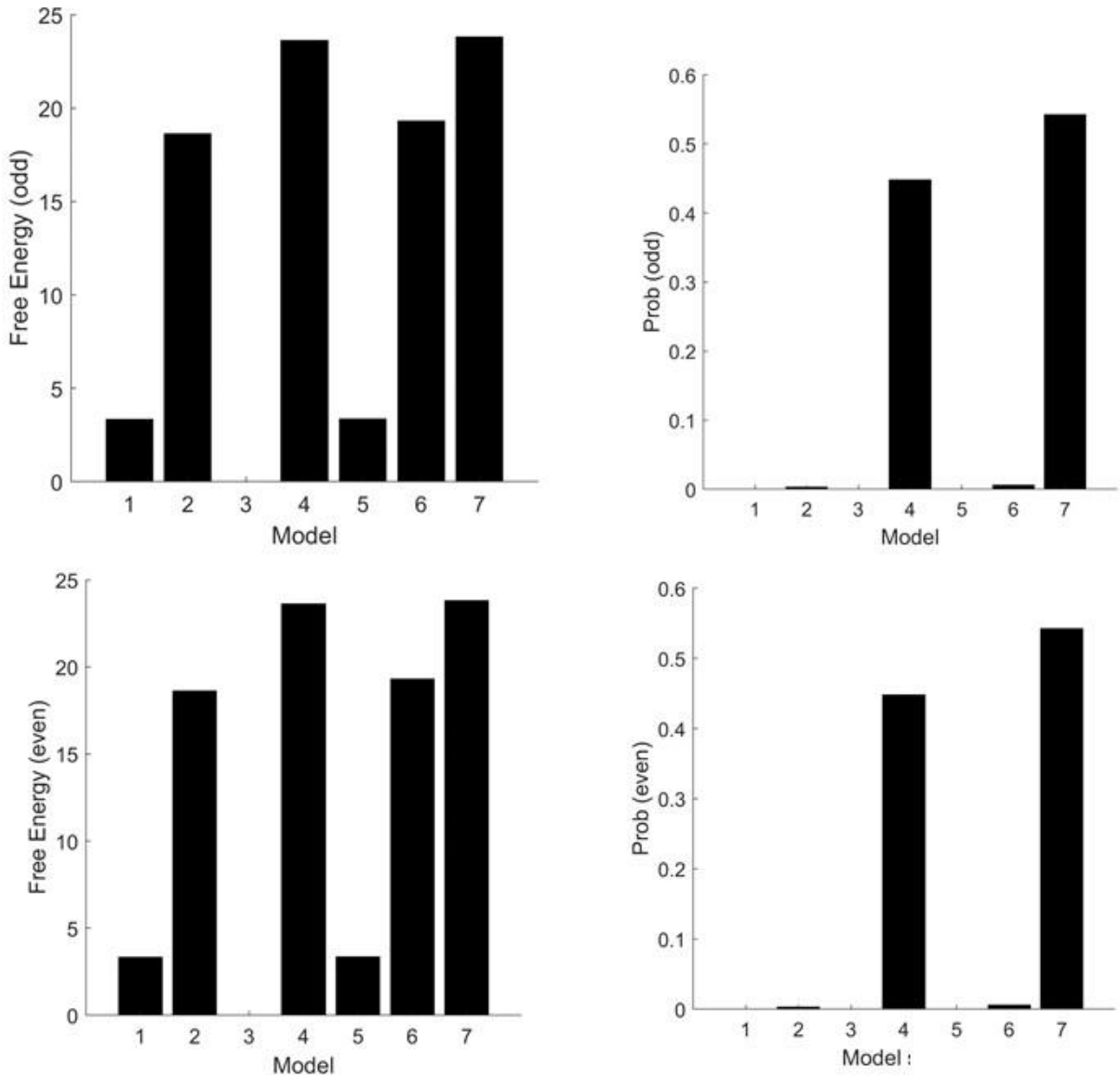

Figure 14. The following figures shows the second level PEB model comparison results with MRS maps (class of first and second order polynomial) as their regressors. . The model comparison associated with different combinations of self-inhibitory connections are at top plot and the model comparison associated with different combinations of inter-regional connections are at the bottom plot.